Key Points:

- Vertical profiles gathered on rockets reveal highly complex, though organized, electrodynamics in the low latitude ionosphere at sunset
- Zonal plasma drifts display shears with altitude, suggesting a vortex pattern, which may establish unstable ionospheric conditions
- Electric field and plasma density measurements on a pair of sounding rockets provide unique measurements in the sunset ionosphere

Correspondence to:

R. Pfaff,
Robert.F.Pfaff@nasa.gov

Author Contributions:

Conceptualization: E. Kudeki
Formal analysis: R. Pfaff, H. Freudenreich, D. Rowland, M. Larsen
Investigation: D. Rowland
Methodology: R. Pfaff, E. Kudeki, M. Larsen
Validation: J. Klenzing
Writing – original draft: R. Pfaff

Dual Sounding Rocket and C/NOFS Satellite Observations of DC Electric Fields and Plasma Density in the Equatorial E- and F-Region Ionosphere at Sunset

R. Pfaff[1] , **E. Kudeki[2]** , **H. Freudenreich[1], D. Rowland[1], M. Larsen[3]** , **and J. Klenzing[1]**

[1]NASA Goddard Space Flight Center, Greenbelt, MD, USA, [2]University of Illinois, Urbana, IL, USA, [3]Clemson University, Clemson, SC, USA

Abstract $\mathbf{E} \times \mathbf{B}$ plasma drifts and plasma number density were measured on two NASA rockets launched simultaneously at sunset from Kwajalein Atoll with apogees of 182 and 331 km, with similar, coincident measurements gathered on the Communications/Navigation Outage Forecasting System (C/NOFS) satellite at 390 km. The combined measurements portray a highly dynamic ionosphere in a narrow range of local time and altitude, providing evidence of vortex-like motions. Although the vertical plasma drift was upwards, its magnitude was not constant, increasing between ~150 and 250 km altitude where the plasma density was reduced. The zonal plasma drifts displayed a shear with altitude, changing from eastward to westward flow below 270 km, coincident with the larger upward drifts and consistent with the maintenance of the vortex flow. The plasma density on the western flank was highly structured compared to the eastern flank, despite the fact that the western region corresponded to slightly earlier local times. These observations illustrate that the low latitude ionosphere at sunset must be considered as an ensemble of interconnected flows encompassing an evolving "theater," as opposed to a background that simply unfolds linearly with respect to local time. The observations also underscore how satellites at high altitudes do not capture the highly dynamic ionosphere and thermosphere at the lower altitudes which are critical for understanding the electrodynamics system. Such motions set the stage for large scale plasma instabilities to form later in the evening, as observed by radars at Kwajalein and subsequent passes of the C/NOFS satellite.

Plain Language Summary Earth's upper atmosphere and ionosphere undergo significant variations between day and night. At sunset, the directions of the ionosphere motions, represented by electric fields, and the upper atmosphere winds, are known to reverse direction at low latitudes. NASA launched two rockets simultaneously with different apogees precisely at sunset from the low latitude launch pad at Kwajalein Atoll to examine how the plasma and neutral dynamics behave during this transitional period. The results reveal a surprisingly complex, though organized, system of flows that change significantly within a very narrow local time period, creating a vortex pattern with respect to altitude and local time. Furthermore, how the low latitude ionosphere evolves within this sunset "theater" is key to understanding how the subsequent nighttime ionosphere might eventually become unstable, creating irregularities responsible for scintillations that disrupt communication and navigation radiowaves.

1. Introduction

The electrodynamics of the equatorial ionosphere has commanded considerable attention among experimentalists, modelers, and theorists since the earliest days of space research. In particular, the motions of the ionospheric plasma at sunset have been studied extensively ever since ionosondes and radar measurements revealed that the equatorial ionosphere often rises rapidly near the dusk terminator (e.g., Fejer et al., 1981; Fejer & Scherliess, 2001; Kelley, 2009). This strong vertical plasma motion is associated with enhanced eastward zonal electric fields and is believed to be an important factor in the initiation of large scale plasma depletions often referred to as equatorial spread-F. In the last 20 yr, the horizontal motions of the plasma have also been identified as playing a key role in the electrodynamics of the sunset ionosphere, led in particular by Jicamarca radar observations (Kudeki & Bhattacharyya, 1999) and satellite observations (Eccles et al., 1999) of plasma vortices in the ionosphere at sunset.

In addition to highly variable plasma drifts in the sunset equatorial ionosphere, neutral upper atmospheric motions or winds are also believed to be an essential ingredient in the overall electrodynamics picture, although direct

measurements of the winds at F-region altitudes at sunset have been elusive. Importantly, Kudeki et al. (2007) demonstrated that differences in the wind and ion drift vectors alone were sufficient to instigate large scale plasma instabilities in the equatorial ionosphere, such as those believed responsible for initiating spread-F. Such conditions are likely encountered at sunset near the magnetic equator, particularly in the presence of vortex patterns in which the neutral gas motions are not expected to mirror those of the coincident plasma.

To test these ideas, comprehensive measurements of vector electric fields (plasma drifts) and winds as a function of altitude gathered in the low latitude sunset ionosphere are necessary. Obtaining these measurements was the aim of the Equatorial Vortex Experiment (EVEX) which is described in the lead article (Kudeki et al., 2022). The present article complements the lead article by describing the *in situ* measurements of the electrodynamic parameters gathered by probes on a pair of rockets launched simultaneously from near the magnetic equator at sunset as well as from a coincident satellite pass in this region. When analyzed in conjunction with the radar and other ground-based measurements, these data help provide the larger scale picture of the evolving ionosphere and neutral atmosphere motions.

Sounding rockets are ideal platforms to gather the necessary data to carry out this scientific research. Not only do they provide largely vertical profiles on relatively slow-moving vehicles, but also, they can be launched directly into regions with desired geophysical conditions known *apriori* in conjunction with detailed ground-based measurements gathered by radars and other instruments. In the case of EVEX, two rockets were launched nearly simultaneously at sunset from Roi Namur, Kwajalein into an ionosphere that was predicted to be unstable, as determined by real-time measurements by the University of Illinois IRIS radar (Kudeki et al., 2022). Furthermore, the experiment was augmented by a perigee pass of the Communications/Navigation Outage Forecasting System (C/NOFS) satellite over the Kwajalein rocket range coincident with the rocket launches, as shown herein.

An outline of this article is as follows: we first describe the dual rocket experiment configuration and the scientific instruments flown on each payload. The data presentation begins with the plasma density and DC electric field measurements from each rocket followed by a data presentation from a simultaneous overfly of the C/NOFS satellite. The $\mathbf{E} \times \mathbf{B}$ drifts from the two sounding rockets and the satellite are presented within composite presentations from which the larger scale electrodynamic picture emerges. Detailed observations of the lower ionosphere "valley" region are then described. The data presentation is followed by a discussion of the overall, large scale sunset electrodynamics of the near-equatorial ionosphere.

2. Experiment Overview

The two NASA rockets from which data are presented here were launched on 7 May 2013, from the Reagan Test Site on the island of Roi Namur (latitude 9°23'49N, longitude 167°28'15E) which is part of the Kwajalein Atoll in the Marshall Islands. The geographic locations of the launch range and the horizontal projections of the two rocket trajectories are shown in Figure 1. As shown here, the launch site at Roi Namur is approximately 4.25° to the north of the magnetic equator. The rockets were launched westward, parallel to the magnetic equator, splashing down about 250 km west of Roi Namur in the Pacific Ocean. The footprint of the orbit of the eastward-moving C/NOFS satellite is also shown in this figure as it executed a pass (orbit 27528) near its perigee of 390 km, slightly to the north of Kwajalein, at precisely the same time as when the rockets were gathering data. Important ground-based scientific instruments, including the VHF backscatter radar, UHF Altair incoherent scatter radar, and AFRL ionosonde, were also located at Roi Namur where they gathered continuous measurements of the ionosphere, prior to, during, and after the rocket launches, as described in the lead article (Kudeki et al., 2022).

The EVEX experiment consisted of two rockets launched 90 s apart such that they were at their respective apogee locations at approximately the same time. The high flyer rocket (NASA 45.005) was launched at 07:39:00 UT (18:52 solar local time) and achieved an apogee of 331 km. The low flyer rocket (NASA 46.001) was launched at 07:40:30 UT (18:53:30 solar local time) and achieved an apogee of 182 km. The trajectories of the two rockets and that of the C/NOFS satellite are shown in Figure 2. The times of the relative positions of the three observing platforms along their respective trajectories are provided at 30 s intervals with respect to 07:40 UT, which was selected as a convenient reference time for the three spacecraft.

Since the experiment was conducted at low latitudes, but off the magnetic equator (as shown in Figure 1), we note here the "apex altitudes" associated with the trajectories shown in Figure 2. Here, we refer to the apex of
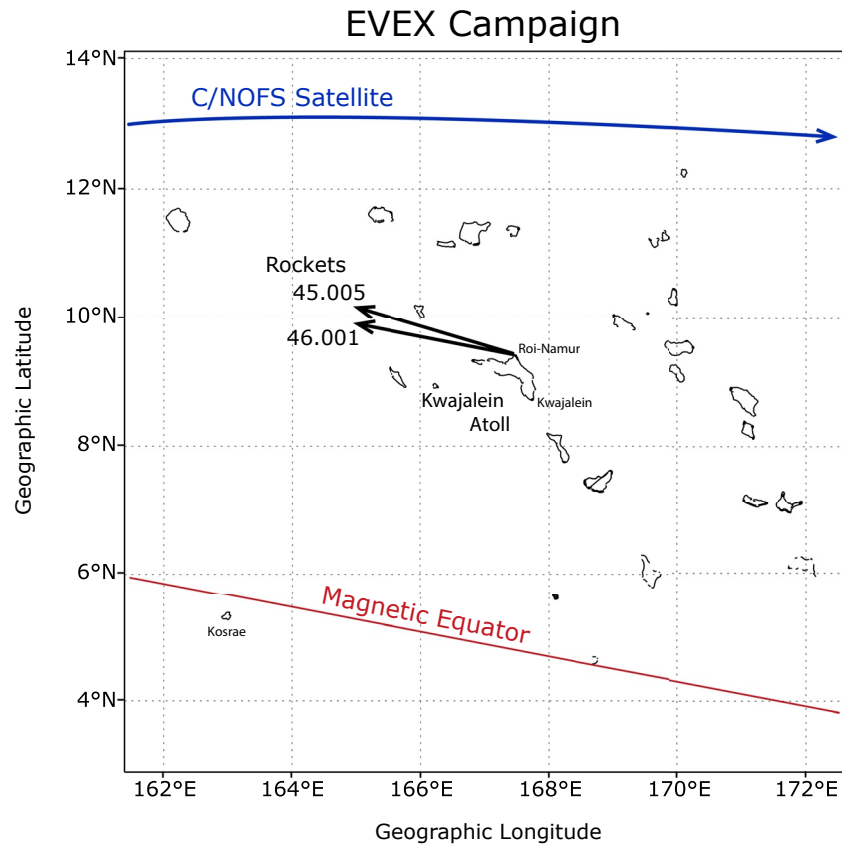
Figure 1. Horizontal trajectories of Equatorial Vortex Experiment (EVEX) rockets 45.005 and 46.001 launched in the western direction from Roi Namur, Kwajalein Atoll. Trajectory of the eastward traveling coincident Communications/ Navigation Outage Forecasting System (C/NOFS) satellite is also shown. The red line shows the location of the magnetic equator.

the dipole magnetic field lines that pierce the payloads at their local measurement altitudes and then rise to their maximum altitudes at the magnetic equator. For C/NOFS, the satellite altitude of ~390 km corresponds to much higher apex altitudes of ~500 km. For the rocket trajectories which are nearer to the magnetic equator and lower in altitude (see Figure 1), the corresponding apex altitudes are only ~40–45 km higher than their actual measurement altitudes, implying that the rockets are generally at or below the field-line-integrated F-region bottomside, and, thus, strongly affected by the field-line-integrated E-region.

Sunset on the ground at Roi Namur occurred at 07:01 UT, although the setting sun was still illuminating the ionosphere above the launch range, including the rocket trajectories, as discussed below. Indeed, as shown by the trajectories in Figure 2, the rockets were launched during the time period in which the lower atmosphere and mesosphere were in shadow and yet the ionosphere was still sunlit, on the verge of coming into darkness.

To fully appreciate the sunset ionosphere conditions in which the rocket probes gathered their data, consider that the sunset terminator at Roi Namur advances westward at approximately 460 m/s, given the rotation speed of the earth at the latitude of Roi Namur (9.5°N). For the EVEX experiment, both of the rockets were launched with horizontal speeds that were somewhat greater than that of the terminator's westward motion: the high flyer (rocket 45.005) had a constant westward velocity of 550 m/s and the low flyer (rocket 46.001) had a constant westward velocity component of 700 m/s. Thus, the rocket trajectories kept the instrument probes largely within the sunset or near sunset conditions for the majority of the data-taking portions of their sub-orbital flights. Furthermore, note that the C/NOFS satellite intersected the longitude of Roi Namur at 07:43 UT. Its velocity at this time was *eastward* at 7,500 m/s at an altitude of 390 km and thus took a horizontal "snapshot" of the ionosphere while the two rocket payloads simultaneously acquired data along their relatively slowly moving parabolic trajectories below.
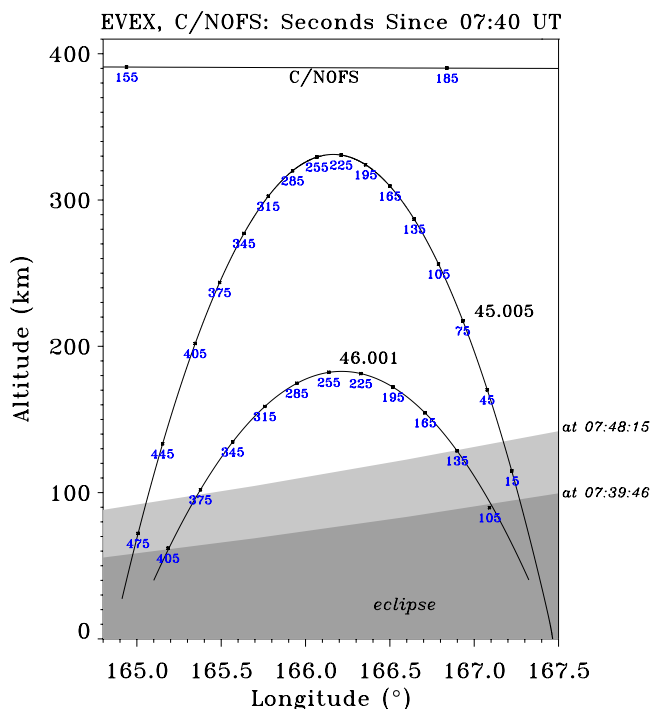
Figure 2. Trajectories of the Equatorial Vortex Experiment (EVEX) rockets, 45.005 and 46.001, and the Communications/Navigation Outage Forecasting System (C/NOFS) satellite in an altitude-longitude format. The small numbers along the trajectories indicate their relative positions at times in seconds since 07:40 UT.

The EVEX experiments consisted of two identical sets of instrumented payloads, as shown in Figure 3, although they included different vapor trail experiments used to illuminate the neutral winds in the E-region ionosphere (rocket 46.001) and F-region ionosphere (rocket 45.005), as described in Kiene et al. (2015). Consistent with the fact that the payloads were flown to significantly different apogees, the launch vehicles used by the two rockets were different: the low flyer used a Terrier Malemute and the high flyer used a Terrier Oriole. From the standpoint of the *in situ* instrumentation, however, the scientific payloads and sub-systems on the two rockets were identical.

The *in situ* instruments on each rocket were comprised of electric field double probes to measure DC and AC fields, magnetometers to measure DC magnetic fields and currents, and Langmuir probes and impedance probes to measure plasma density, all provided by NASA/GSFC. The instrument configuration on the payloads is shown in Figure 3. DC and AC electric fields were gathered with a pair of 5 m (tip-to-tip) orthogonal double probes extended about the spin axis that included dual spheres configured to enhance the measurement of the DC electric fields as well as to enable plasma wave interferometry measurements. The inner spheres were located 0.75 m inboard of the outer spheres. The geometry of the electric field probes is shown in Figure 4, with the electric field spheres labeled, 1–8.

An attitude control system was included on each payload to orient the spin axis along the magnetic field direction and to control the payload spin rate. Orienting the spin axis along the magnetic field direction enabled the two orthogonal double probes in the spin plane to completely specify the vector DC and AC electric fields based on the very good assumption that there are no electric fields along the magnetic field direction, or that $\mathbf{E} \cdot \mathbf{B} = 0$. Attitude knowledge of the payload was provided by a gyro and was accurate to better
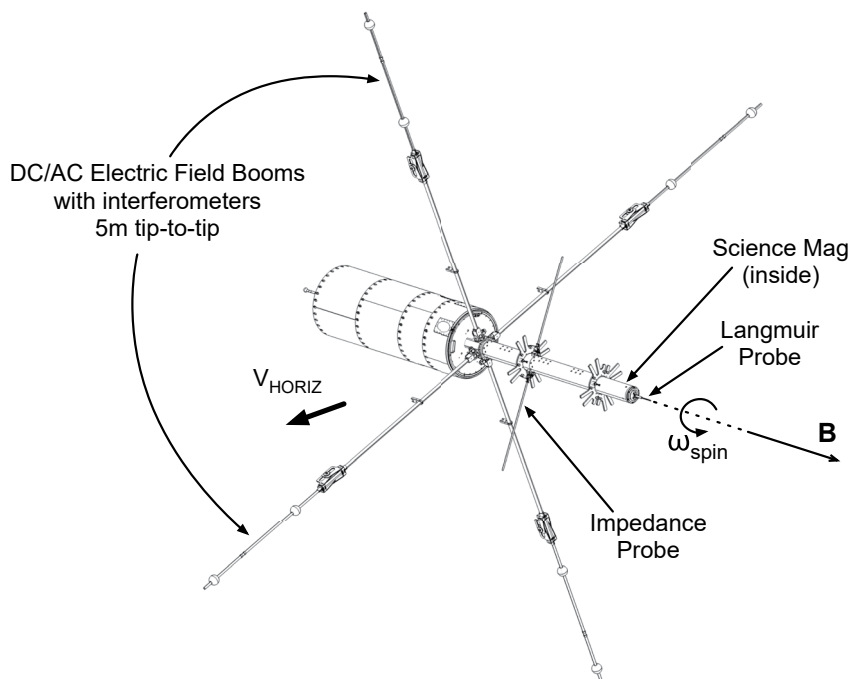

Figure 3. Sketch of payload 45.005 showing orientation of the electric field booms in the spin plane and position of Langmuir probe along the spin axis and flux-gate magnetometer (inside the central tube away from the main payload.) Payload 46.001 had an identical instrument configuration.
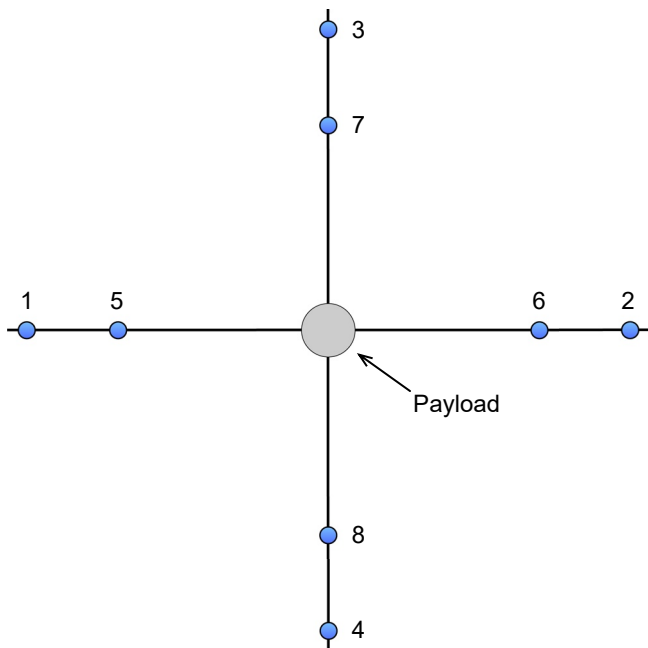
Figure 4. Sketch showing the orthogonal, 5 m tip-to-tip electric field booms in the spin plane and position of the outer spheres, numbered 1–4. The inner spheres, numbered 5–8, were positioned 0.75 m inboard of the outer spheres.

than 1°. Below, we discuss how additional attitude information, obtained from the solar photoelectron "shadow pulses" in the electric field data which occur as one sphere of each double probe pair rotated into the payload shadow once per spin, were used to further refine the attitude solutions. Note that the spin axis was oriented within a few degrees of the magnetic field for the majority of both flights, with this angle increasing to about 5° during the downleg at the lowest altitudes (∼100 km) where the payloads were still gathering meaningful data. The rocket payloads included a GPS system for accurate positional, and hence, velocity, information from which the $\mathbf{V} \times \mathbf{B}$ contributions to the measured electric fields could be accurately determined and subtracted from the measured potential differences, as discussed below.

Clear skies were an important launch condition that was required to enable the wind velocities to be ascertained by the vapor trail experiments released by each rocket, as described by Kiene et al. (2015) and discussed in the lead article (Kudeki et al., 2022).

Ground-based observations at Roi Namur formed an essential part of the EVEX experiment. These included UHF incoherent scatter radar measurements, VHF backscatter measurements, and ionosonde measurements which are described in the lead article (Kudeki et al., 2022).

3. Data Gathered With *In Situ* Probes on the Rockets

We now present the measurements gathered by the *in situ* probes on both rockets. We begin with the plasma density data gathered by both rockets, as that sets the stage for the DC electric field data which are then presented sequentially for the high flyer and low flyer rockets.

3.1. Plasma Density Measurements

On both rockets, the plasma density was continuously measured along each trajectory with two Langmuir probes and an impedance probe.

The Langmuir probes, which were designed to measure the ambient plasma density and its variations as well as electron temperature, consisted of two separate, independent probes which were extended along the spin axis in the forward and aft locations on the payload, as shown in Figure 3. Since the payload flew basically on its side with the spin axis aligned with the magnetic field direction, the two Langmuir probes, each extended along the spin axis at either end of the payload, were oriented essentially perpendicular to the rocket velocity vector.

The aft Langmuir probe had a spherical sensor (2.5 cm diameter) and was biased with a constant −5 V bias. Current collected from this "fixed bias" probe provided very high time resolution measurements of the ambient ion number density and its variations, sampled at 8 ksamples/s. A cylindrical Langmuir probe on the forward end of the payload consisted of an active cylindrical element that was 3 cm long and 0.25 cm in diameter, extended on a support rod of 10 cm length and a diameter of 0.25 cm that was biased at the same voltage as the active sensor to minimize stray current contributions. The tip sensor was swept (with 250 msec ramps) from −5 to 5 V every 5 s to provide electron temperature and spacecraft potential information (presented elsewhere).

In Figure 5, the plasma density from the Langmuir probe instruments are superimposed for each payload plotted vs. altitude, with the upleg data for both rockets in panel (a) and the downleg data in panel (b). The density data from the two rockets were normalized at their apogees using the ionosonde data in conjunction with information from the on-board impedance probe data (see Appendix A).

The plasma density profiles in Figure 5 clearly indicate that the lower ionosphere was beginning to show effects of recombination as the EUV source function was disappearing with the setting sun. There is a smooth, yet distinct decrease in the plasma density below 250 km, the altitude we associate with the F-region ledge (which was corroborated with radar and ionosonde data). Further below, the plasma density continues to decrease
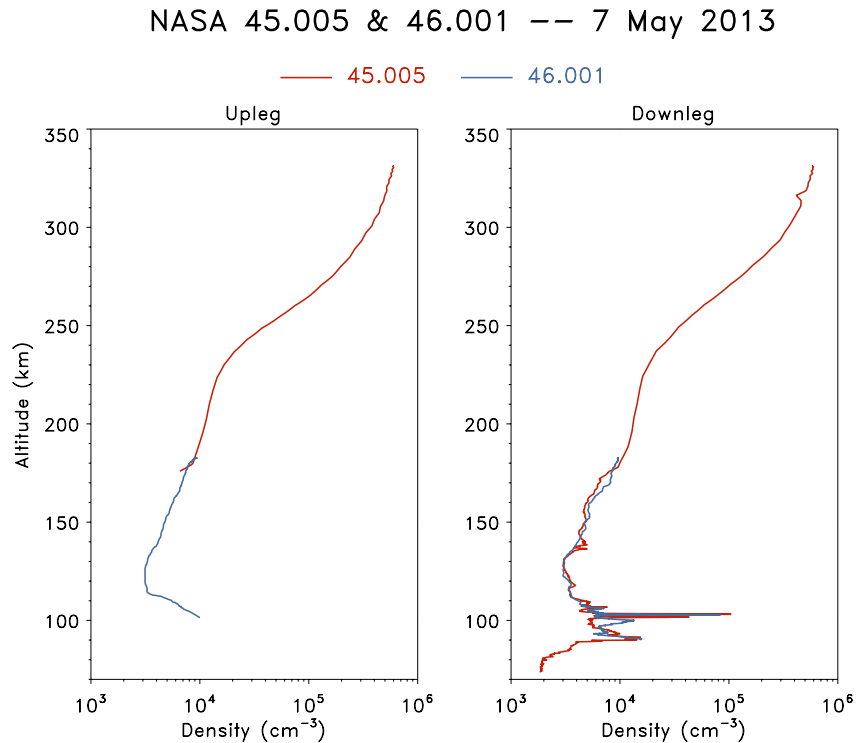
Figure 5. Plasma density measured by probes on the 45.005 (high-flyer) and 46.001 (low-flyer) payloads plotted vs. altitude for the upleg and downleg.

slightly with altitude until it encounters another gentler ledge or "knee" in the altitude profile around 180 km which is particularly apparent in the downleg data. Below this, the density falls off more rapidly since recombination effects are more effective at the lower altitudes due to the increase in the abundance of molecular ions in the E-region. Notice further that at the base of the ionosphere at lower altitudes (90–110 km), the plasma density increases somewhat. This increase in the lower E-region may be associated with plasma motions and wind-driven forcing, although it may also be enhanced due to a greater abundance of metallic ions at these altitudes, which do not recombine as quickly. The lower E-region ionosphere is also observed to be more structured, particularly on the downleg of each rocket, where both payloads encountered sporadic-E layers. We discuss the plasma density structure further on below.

Before continuing we note that the sharp, localized decrease in observed plasma density near 320 km on the downleg of rocket 45.005 that resembles a small "notch" in Figure 5 is due to the perturbation of the ambient density responding to the vapor trail release and is not of geophysical origin.

3.2. DC Electric Field Measurements—High Flyer Rocket

We turn now to the DC electric field measurements. Examples of the DC electric field data from two perpendicular double probes gathered on the downleg of the high flyer rocket (45.005) near 220 km altitude (at 454 s after launch), are shown in the spacecraft frame in Figure 6. The outermost, opposite spheres formed the main orthogonal measurements, such that the potential differences between spheres 1 and 2 provided the "E12" component (upper two panels) and the potential differences between spheres 3 and 4 provided the orthogonal, "E34" component (lower two panels). The large sine waves occur at the payload spin period of roughly 2 s. Gathered with 6 cm diameter spherical sensors with a Titanium Nitride coating, these fields represent the measured potentials divided by their 5 m (tip-to-tip) boomlengths. Notice that the electric field magnitudes are the same for the two components yet their phases differ by 90° as expected for orthogonal double probes deployed in the payload spin plane.
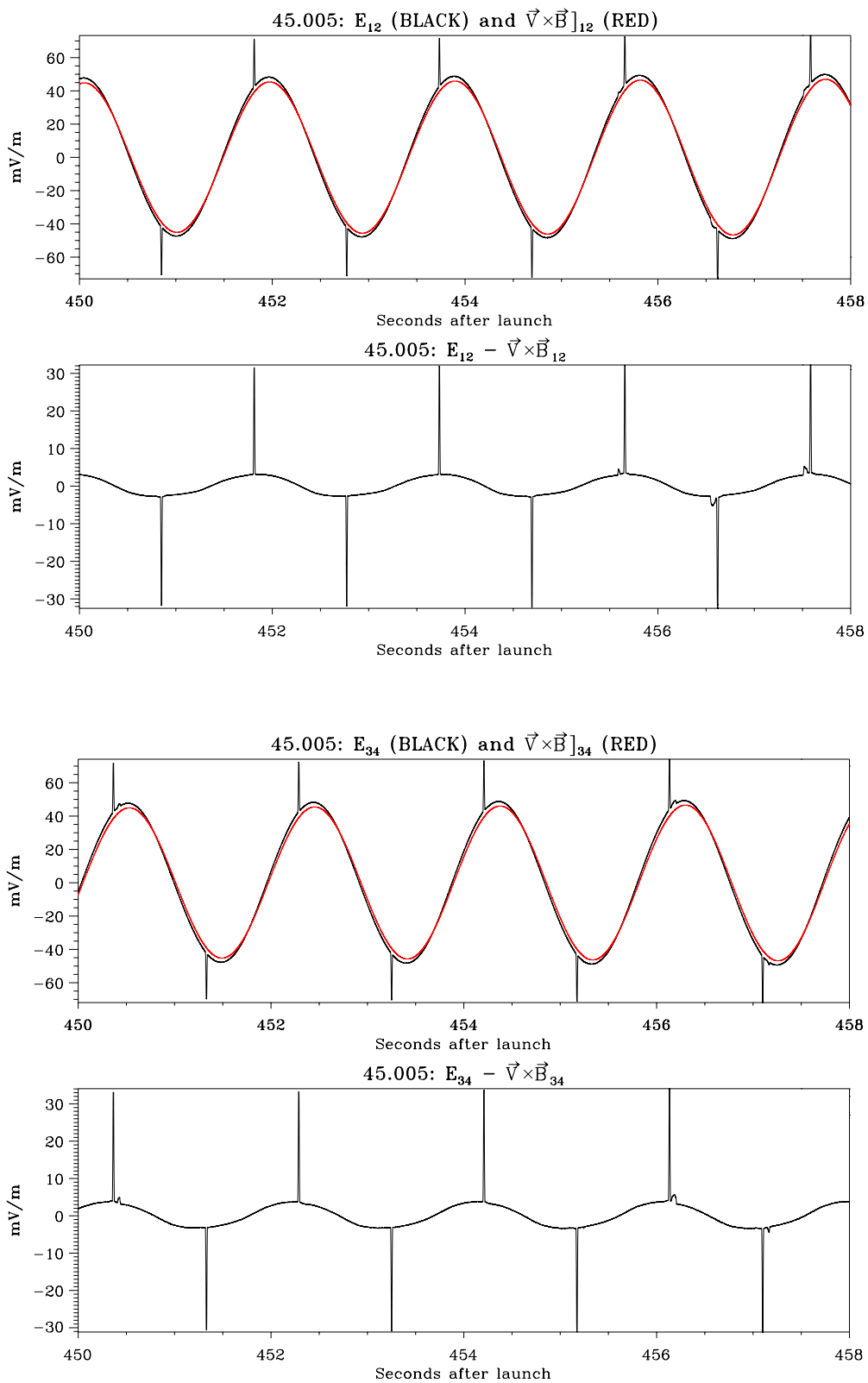
Figure 6.

The largest contribution to the electric field measurement on a spacecraft moving through the equatorial ionosphere is that due to the $\mathbf{V} \times \mathbf{B}$ fields created by the motion of the payload across the Earth's ambient magnetic field, where $\mathbf{V}$ is the spacecraft velocity in the earth-fixed frame and $\mathbf{B}$ is the ambient magnetic field. The calculated contributions due to $\mathbf{V} \times \mathbf{B}$ along each component are shown by the red curves in the upper portions of each pair of panels in Figure 6 and represent the fields that would have been measured if no ambient (i.e., geophysical) electric fields were present. Our next step is to subtract these $\mathbf{V} \times \mathbf{B}$ fields from the measurements, which is shown in the bottom portion of each pair of panels of Figure 6 corresponding to the two perpendicular components. We then rotate the resulting components from the spacecraft frame into a geophysical coordinate system in order to interpret the results.

Before proceeding, we comment on the appearance of sun "shadow pulses" in the raw electric field data which occur twice per spin and are especially prominent in the data shown in Figure 6. These notches are due to photoelectron current asymmetries which occur when one sphere of each double probe pair rotates into the shadow of the payload while the opposing sphere is in sunlight. The sun pulses also provide independent attitude information. Since this rocket was launched at sunset, the sun was near the horizon and hence the spikes occur near to that part of the spin cycle when each boom pair rotated through the horizontal direction with one sphere (of each pair) occulted by the shadow of the main payload. Indeed, when we inspect the difference curves of the E12 and E34 measured fields in the lower portions of each panel pair of Figure 6, we see that the sun spikes are essentially in the center of a smaller amplitude sine wave at the spin frequency which generally peaks at the same times as the appearance of the sun notches. As will be shown immediately below, the ambient DC electric fields at this time were almost entirely in the zonal (east-west) direction (see DC electric fields corresponding to a flight time of 454 s in next figure) consistent with the presence of the sun pulses which occurred when the booms rotated through the near horizontal direction, since the sun was setting.

The difference fields (measured fields minus $\mathbf{V} \times \mathbf{B}$ for each component) are rotated into geomagnetic coordinates and plotted vs. time for the high flyer rocket (45.005) in Figure 7. Here, the meridional fields are shown in the uppermost panel and the zonal fields are plotted in the panel below that. The zonal fields correspond to the magnetic east-west direction (+ is East) and the meridional fields are essentially up-down (+ is Up) as this component is perpendicular to the zonal direction and to the magnetic field direction which is essentially north-south. The vector electric fields are depicted as "needle plots" in the second panel from the bottom and the $\mathbf{E} \times \mathbf{B}$ plasma drifts associated with these fields are plotted as needle plots in the lowest panel. Notice in Figure 7 that the zonal electric fields (second panel from the top) are in the eastward direction throughout the flight, indicative of upwards or vertical plasma drifts at all altitudes encountered by the rocket. These eastward fields are stronger during the downleg, associated with the lower plasma density of the upper "valley" region of the rapidly recombining ionosphere below the F-region ledge, as discussed below. On the other hand, the vertical drifts actually diminish below about 140 km where the plasma density decreases further, as was also observed on the low flyer (presented in the next sub-section).

The meridional electric fields show significant variations in both amplitude and direction throughout the flight, basically depicting downward fields (eastward flows) for the middle portion of the flight, from approximately 200 km (~130 s) on the upleg, through apogee and continuing until the rocket was at approximately 270 km (~420 s) on the downleg, at which time the ambient meridional electric fields shifted to upwards (corresponding to westward plasma drifts).

To better illustrate how the plasma drifts change with altitude and appear, to some extent, organized by the plasma density, the $\mathbf{E} \times \mathbf{B}$ velocities shown in Figure 7 are now plotted vs. altitude for the upleg and downleg of rocket 45.005 in Figure 8. In this figure, we also show the plasma density measurements in the left-hand panel that were discussed above with respect to Figure 5.

The middle panel of Figure 8 shows how the meridional or near-vertical plasma drift components are upwards throughout the flight, as shown in the upleg and downleg data. The amplitudes are quite small (~20 m/s) near

Figure 6. Upper panels show 8 s of raw data from two orthogonal, 5 m tip-to-tip electric field double probes in the spin plane of rocket 45.005 when that rocket was near 250 km on the downleg and the measured field was mostly eastward. The superimposed red curves show the calculated fields due to the $\mathbf{V} \times \mathbf{B}$ motion of the payload across the earth's ambient magnetic field. The difference of these curves are shown in the lower panels and represent the geophysical fields of interest, in the frame of reference of the spinning payload. The narrow spikes represent photoelectron currents when one probe rotates into the shadow of the main payload, as explained in the text.
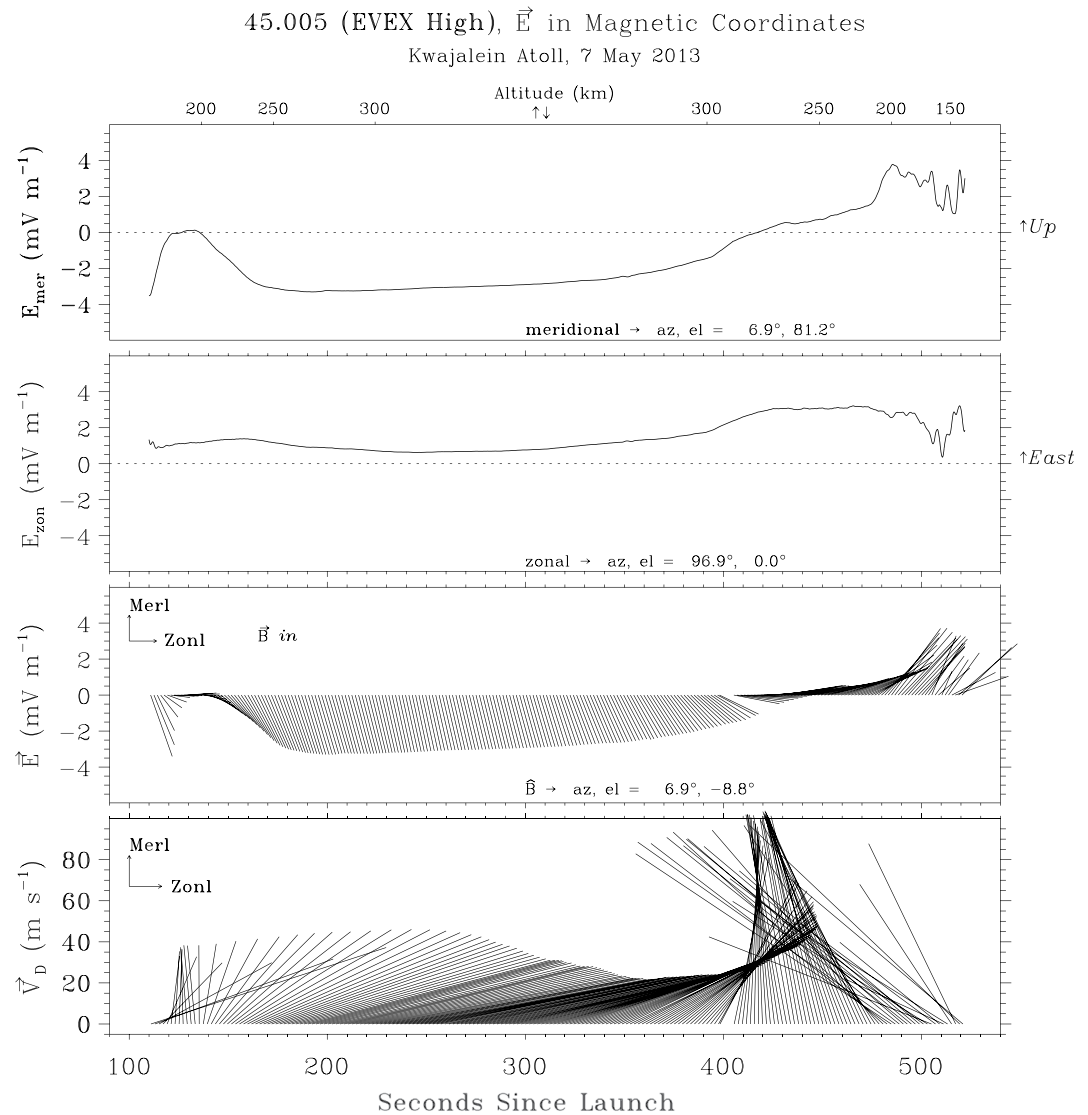
Figure 7. Electric field measurements from the double probes gathered during the flight of rocket 45.005. The top two panels show the electric fields in the meridional and zonal directions. The second panel from the bottom shows the vector electric field (perpendicular to the magnetic field) in arrow plot display. The lowest panel shows the $\mathbf{E} \times \mathbf{B}$ plasma drifts in a similar arrow plot display corresponding to the measured electric fields.

apogee of 330 km where the plasma density is largest $\sim 5 \times 10^6$ cm^{-3} yet increase markedly below about 270 km where the plasma density falls off corresponding to an evolving and gradual ledge of the sunset F-region. That the vertical drifts are so large (~ 100 m/s) on the downleg is surprising compared to the smaller amplitude drifts customarily measured by the Jicamarca incoherent scatter radar near 200 km altitude (Fejer et al., 2014). Nevertheless, the increased vertical drifts coincident with a region of altitude broadly associated with lower plasma density is unmistakable. Such fields may be associated with strong neutral winds and the need for current continuity in the evolving plasma dynamics, as discussed later.

The zonal drifts also show a significant difference between the upleg and downleg and a remarkable variation with altitude accentuated by considerable horizontal shear flow within narrow altitude regimes. Indeed, as mentioned above, the plasma drift shifts from eastward to westward on the downleg near 270 km where the plasma density changes considerably. The westward plasma velocity increases in amplitude to about 100 m/s in the region from 130 to 170 km on the downleg and is generally consistent with radar line-of-sight measurements that show westward plasma motions in the E-region at these altitudes, as discussed in the lead article (Kudeki
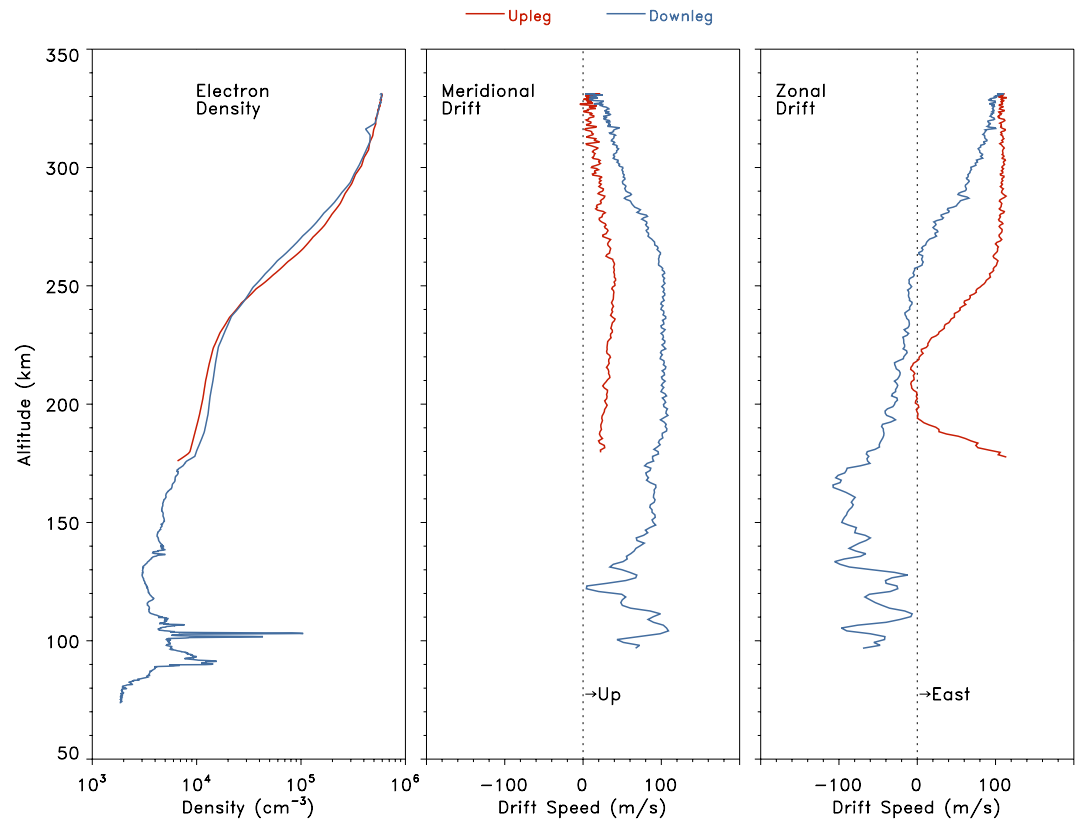
Figure 8. Plasma density and $\mathbf{E} \times \mathbf{B}$ plasma drift measurements plotted vs. altitude for the upleg and downleg trajectories of rocket 45.005. The density data are shown in the left panel, the meridional drifts are shown in the center panel, and the zonal drifts are shown in the right panel. Upleg measurements are not available below approximately 180 km altitude as the instruments and payload orientation are being prepared for data gathering during this initial portion of the flight.

et al., 2022). The upleg zonal drifts show steady eastward flow between 270 and 330 km (apogee), yet decrease to much lower speeds below 250 km, becoming slightly westward near 200 km, before increasing to larger, eastward velocities for a brief interval below this altitude.

Note that E-region measurements were not available for the upleg below about 170 km, given its higher apogee and need to deploy the nosecone and booms on the upleg while the payload traversed the lower ionosphere with a very large upwards velocity. Both the meridional and zonal components become somewhat more structured on the downleg near the end of the flight in the E-region, as discussed further on below.

3.3. DC Electric Field Measurements—Low Flyer Rocket

Similar presentations of the measured DC electric fields and associated plasma drifts for the low flyer rocket (46.001) are now provided. For this rocket, unfortunately, one of the four electric field booms did not completely deploy (in this case, the boom with spheres #1 and #5, see Figure 4). Fortunately, data from the other spheres are good and provide the vector DC electric fields presented here for this rocket. Since one boom did not fully deploy, electric field "solutions" for the low flyer rocket were created in two ways. First, we calculate the DC vector electric fields at the times of the peaks of the one boom pair that fully deployed, the E34 component, twice per spin period. Since this component was maximized at these peaks, the corresponding orthogonal measurement would measure no electric fields at this time. Knowing the precise orientation of the E34 component at the times of these peaks, this approach provides a full vector solution twice per spin, corresponding to the two measured
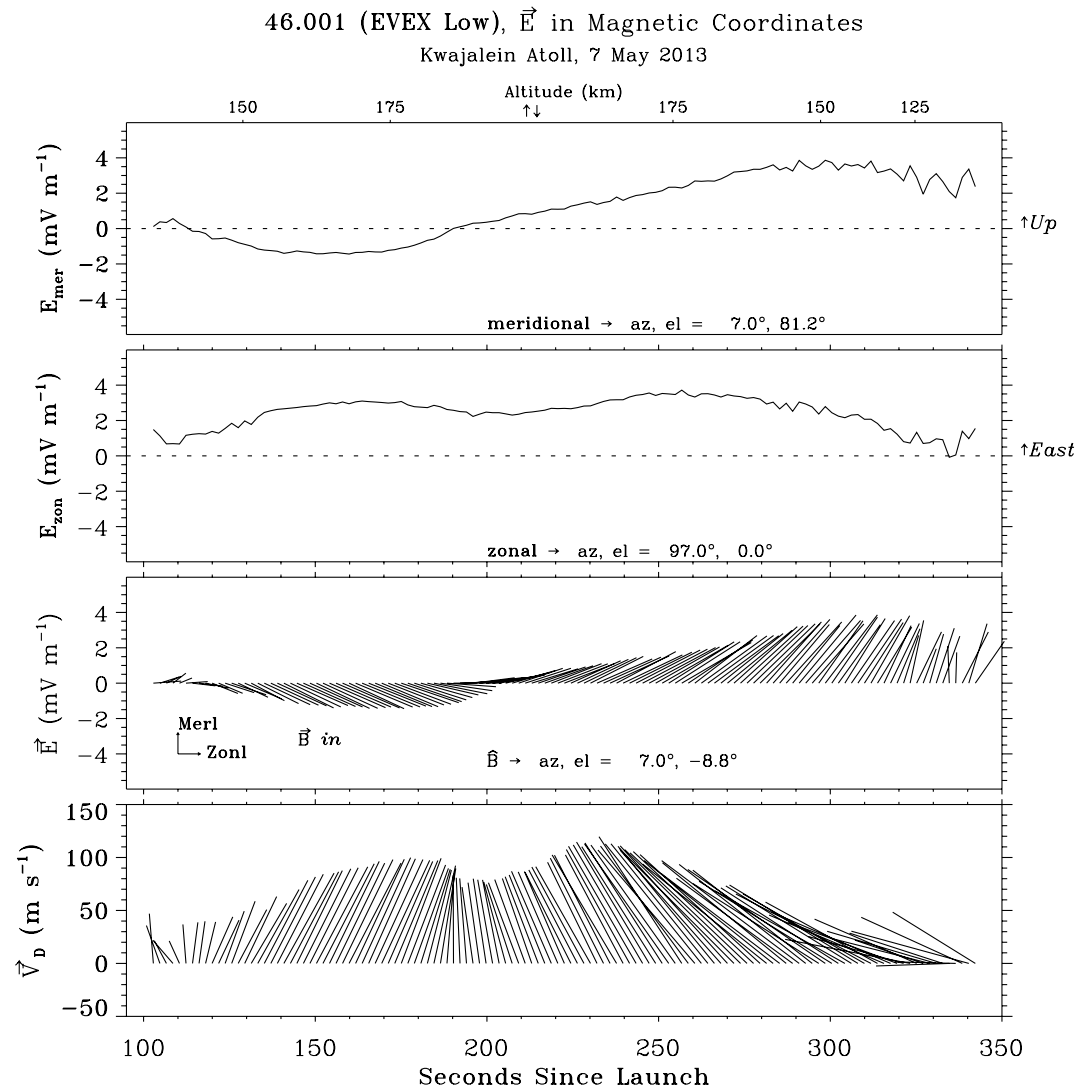
Figure 9. Electric field measurements from the double probes gathered during the flight of rocket 46.001. The top two panels show the electric fields in the meridional and zonal directions. The second panel from the bottom shows the vector electric field (perpendicular to the magnetic field) in arrow plot display. The lowest panel shows the $\mathbf{E} \times \mathbf{B}$ plasma drifts in a similar arrow plot display corresponding to the measured electric fields.

sine wave peaks observed within each payload spin. We also calculated the instantaneous vector electric fields from combining the orthogonal "diagonal" double probe pairs formed by spheres 2 and 3 (the E23 component) and spheres 2 and 4 (the E24 component). Both solutions provided similar results. We show results from the combined E23 and E24 data in Figure 9 as their continuous measurements (i.e., not limited to the peaks of the spin cycle sine wave) provide higher time resolution vector measurements.

The ambient DC electric fields (and associated $\mathbf{E} \times \mathbf{B}$ drifts) measured by probes on the low flyer rocket (46.001) shown in Figure 9 are similar in many ways to the electric fields measured by the high flyer. Again, the zonal electric field component was mostly eastward for the entire flight, with slightly smaller values near apogee, perhaps because this payload encountered larger ambient plasma density at this time. On the other hand, the meridional electric fields (zonal drifts) varied significantly between the upleg and downleg, indicative of the fact that the zonal drifts were undergoing significant spatial and temporal variations during this rapidly changing sunset ionosphere, exhibiting largely eastward drifts on the upleg which shifted to westward drifts during the downleg.
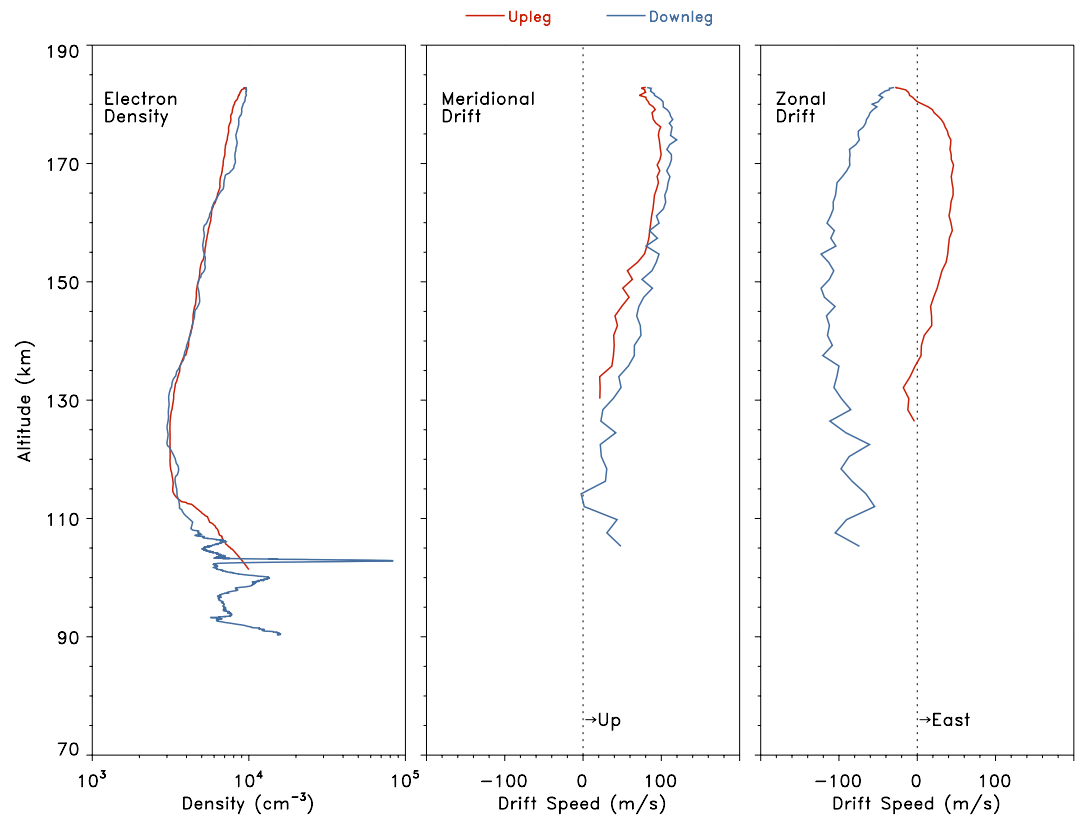
Figure 10. Plasma density and $\mathbf{E} \times \mathbf{B}$ plasma drift measurements plotted vs. altitude for the upleg and downleg trajectories of rocket 46.001. The density data are shown in the left panel, the meridional drifts are shown in the center panel, and the zonal drifts are shown in the right panel. Upleg measurements are not available below approximately 130 km altitude as the instruments and payload orientation are being prepared for data gathering during this initial portion of the flight.

The altitude variations of the drifts are shown in Figure 10, plotted alongside the plasma density data for the upleg and downleg, in the same format as in Figure 8 for the high flyer rocket. As for the high flyer rocket, although the upleg and downleg portions of the rocket trajectory corresponded to the same altitudes, the horizontal portion of the trajectories during these times corresponded to different longitudes and local times that were characterized, at least in this experiment, by very different zonal $\mathbf{E} \times \mathbf{B}$ drifts. Notice that the meridional drifts were essentially upward through the upleg and downleg, yet were significantly larger above about 150 km altitude. That the downleg upward drifts reached amplitudes of near 100 m/s is consistent with the high flyer measurements at these altitudes.

In this case, however, the drifts measured on the upleg were also quite large (~80 m/s) in this altitude region, yet lower than the downleg. Note that the upwards plasma drifts did not increase near 130 km where the plasma density decreased to its lowest values ($2–5 \times 10^4$ cm^{-3}). The zonal drifts observed on the low flyer rocket (right-hand panel of Figure 10) displayed significant variations with altitude, with predominantly eastward flow on the upleg and westward flow on the downleg. We interpret these highly dynamic plasma variations as indicative of the shear and dramatically changing conditions at sunset, which are at the core of the EVEX experiment, as discussed further on below.

Similar to the high flyer, note that lowest altitude measurements below about 130 km were not available on the upleg for this rocket, given the need to deploy the nosecone and electric field booms on the upleg. Finally, notice the large scale structure of the DC electric fields, particularly on the downleg below 130 km. We will also return to this below.
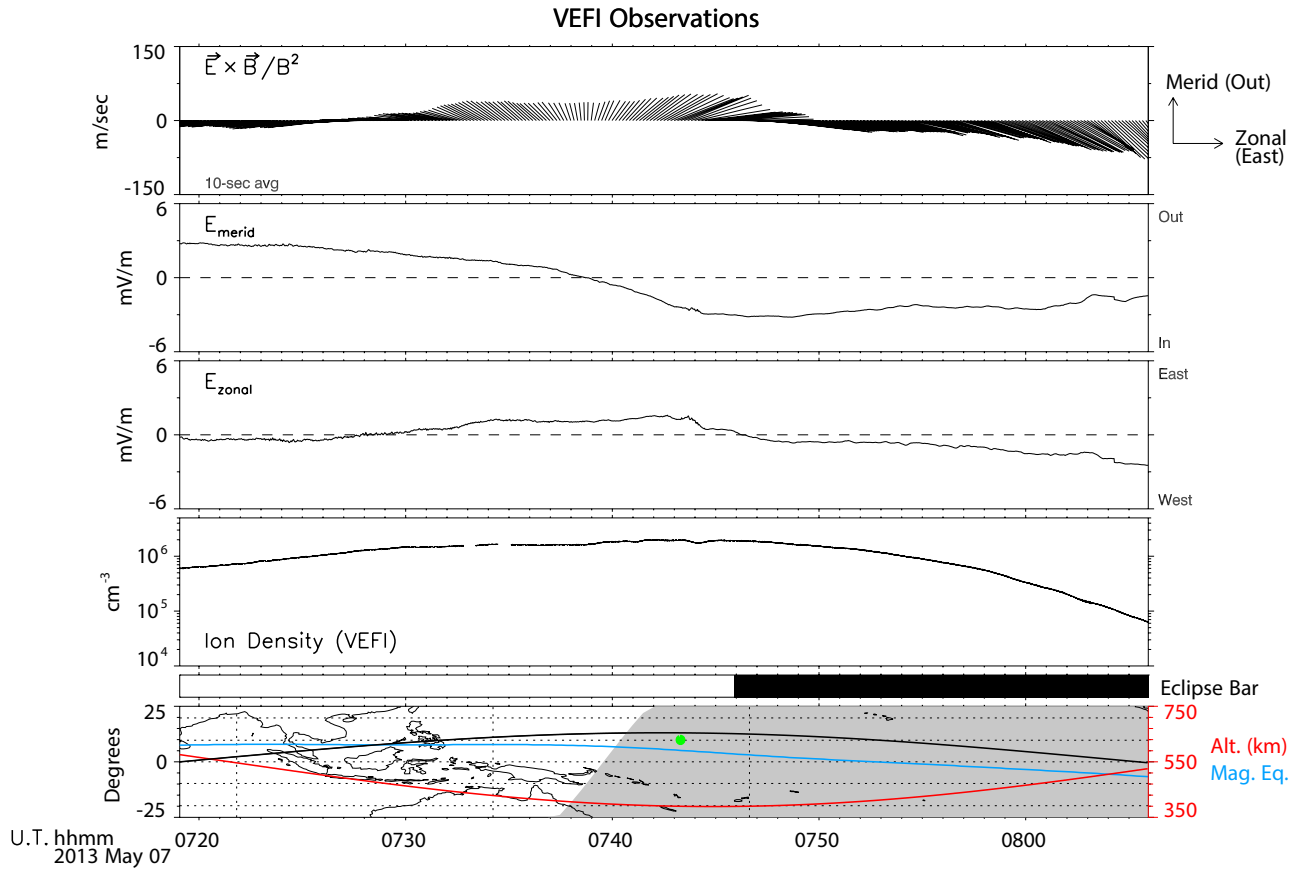
Figure 11. Vector DC electric fields, associated **E × B** plasma drifts, and plasma number density gathered on the Communications/Navigation Outage Forecasting System (C/NOFS) satellite during an overflight of Kwajalein that was coincident with the launches of the two EVEX rockets. The second and third panels show the meridional and zonal electric field observations while the uppermost panels show their corresponding E × B drifts in an arrow display. The fourth panel shows the plasma density measured along the satellite trajectory as measured with the fixed-bias Langmuir probe. The lowest panel shows the geographic location of the satellite, depicted by the black line as well as its altitude, depicted by the red line. The blue line shows the location of the magnetic equator for reference, and the gray shading shows the location of the earth's shadow on the ground. The black line in the "eclipse bar" shows when the satellite was in the earth's shadow. The green dot shows the location of the Kwajalein rocket range.

4. C/NOFS Satellite Observations

We now present DC electric field and plasma density measurements gathered on the C/NOFS satellite as it executed perigee passes above Kwajalein on 7 May 2013 at 7:43:00 UT. As shown in Figure 11, data from the first pass (orbit 27,528), which was coincident with the rocket launches, show the meridional and zonal components of the DC electric field in panels 2 and 3 (from the top). The electric field data were gathered with the Vector Electric Field Investigation (VEFI) sensors for which the instrument and data processing are described in Pfaff et al. (2010). The top panel shows a needle plot of the **E × B** velocities associated with these measured DC electric fields. The lowest data panel shows the density measured by the VEFI Langmuir Probe. Below this is an indicator (the "eclipse bar") showing when the spacecraft was illuminated and when it was in the earth's shadow.

In the lowest panel of Figure 11, there is a map of the low latitude region in which the "footprint" of the C/NOFS orbit is shown by the black line. The altitude of C/NOFS is shown in red and indicates that the satellite was at its perigee of 390 km near 07:43 UT as it passed closest to Kwajalein whose location is depicted by a green dot. As shown here and previously in Figure 1, the satellite passed about three degrees north of Kwajalein. Finally, the magnetic equator is shown in blue for reference.

Notice that the zonal electric fields are slightly enhanced near 07:42 UT, just after sunset on the ground and just prior to the satellite entering eclipse. This increase in the vertical (upwards) directed plasma drift represents the

"pre-reversal" enhancement, as the direction of the zonal electric field reversed direction and turned westward at later times, corresponding to downward vertical plasma flow after this brief increase of the upwards velocity.

The meridional electric fields (corresponding to zonal drifts) changed sign prior to sunset and somewhat prior to the pre-reversal enhancement in the zonal electric field. For this orbit, the change of sign of the meridional electric field occurred near 07:39 UT when the satellite was approximately 2,000 km to the west of Kwajalein at about 400 km altitude. This change in meridional electric fields or zonal plasma drifts corresponds to the typical late afternoon local time for the diurnal switch from westward to eastward flow in the F-region near 400 km altitude, as shown by numerous satellite studies (see, e.g., Coley et al., 2014; Fejer et al., 2013).

For this pass of the C/NOFS satellite, the plasma density measured by the satellite probe remained relatively unstructured throughout this time period. (Interference from the satellite torque rods is observed near 07:33–07:35 UT.) There is a hint of a very small plasma undulation developing just to the east of the Kwajalein location near 07:44 UT with some coincident electric field fine structure, which corresponded to the sharp decrease of the zonal electric field amplitude. These very small electric field variations may possibly be significant, but we note that electric field variations with similar magnitude were observed during other portions of the orbit as well.

The data from the subsequent C/NOFS pass (102 min later), however, revealed two large density depletions that had developed over Kwajalein within this time interval. These are very clear in the middle panel of Figure 12 which shows the plasma density from three consecutive C/NOFS passes over Kwajalein. Here, the density data in the top portion of the figure corresponds to that shown previously in Figure 11, whereas the middle and lower data panels correspond to C/NOFS passes 102 and 204 min later. The large density depletions over Kwajalein are indicative of "Spread-F" processes, observed in the Altair radar and ionosonde and which are discussed in the lead article (Kudeki et al., 2022) may have "grown" from two negative excursions within this packet of large scale density modulation. The lowest panel turning to the plasma density in the middle panel of Figure 12 over the Kwajalein region (between ~160° and 175° longitude), notice that the continuous plasma density measurements along the orbit reveal large scale structures prior to, and in between, the two large density depletions. This strong modulation corresponds to scale sizes of roughly 100–200 km (along the orbit track) which includes the width of the observed sharp density depletions. In fact, the data suggest that the two large depletions present the plasma density gathered on the next pass. Here, the largest depletions are somewhat subdued in their relative depth, without evidence of the modulation of the ambient density between the depletions. The two depletions over Kwajalein in the lowest panel appear to be the same as those in the middle panel, as they have almost an identical horizontal spacing. However, they have shifted eastward, corresponding to an eastward drift speed of ~110 m/s, similar to the $\mathbf{E} \times \mathbf{B}$ zonal drift component associated with the meridional electric field amplitude measured at this time, as shown in Figure 11. The plasma density data from the third orbit (lowest panel of Figure 12) also presents new spread-F depletions to the west of Kwajalein, which are "fresher" as they are correspond to the local sunset region corresponding to this orbit. These spread-F depletions are also manifest in the Altair radar data, as discussed in the companion article (Kudeki et al., 2022).

5. Consolidated Measurements

Our next step is to consolidate the simultaneous, synergistic plasma measurements gathered by the probes on the two EVEX rockets and the C/NOFS satellite, mindful of limitations of combining space and time in what are inherently measurements along one-dimensional trajectories.

The plasma density and $\mathbf{E} \times \mathbf{B}$ drifts measured by probes on the downleg of the two rockets are overlaid and plotted vs. altitude in Figure 13, showing the traversals of the E-region and lower F-region ionosphere. The neutral wind velocities gathered from the high and low altitude vapor trails are also shown (Kiene et al., 2015). The F-region wind measurements are derived from the motion of the lithium tracers and have an uncertainty of +/−15 m/s. The E-region wind measurements are derived from the TMA (trimethyl aluminum) trail motions and have an uncertainty of +/−10 m/s. The neutral wind measurements and their uncertainties are described in detail in Kiene et al. (2015).

The $\mathbf{E} \times \mathbf{B}$ plasma drifts associated with the DC electric fields measured along the rockets' parabolic trajectories yet displayed here vs. altitude show general agreement between the two data sets, with considerable variability present in both $\mathbf{E} \times \mathbf{B}$ components, as well as the plasma density below about 160 km. As mentioned earlier, an
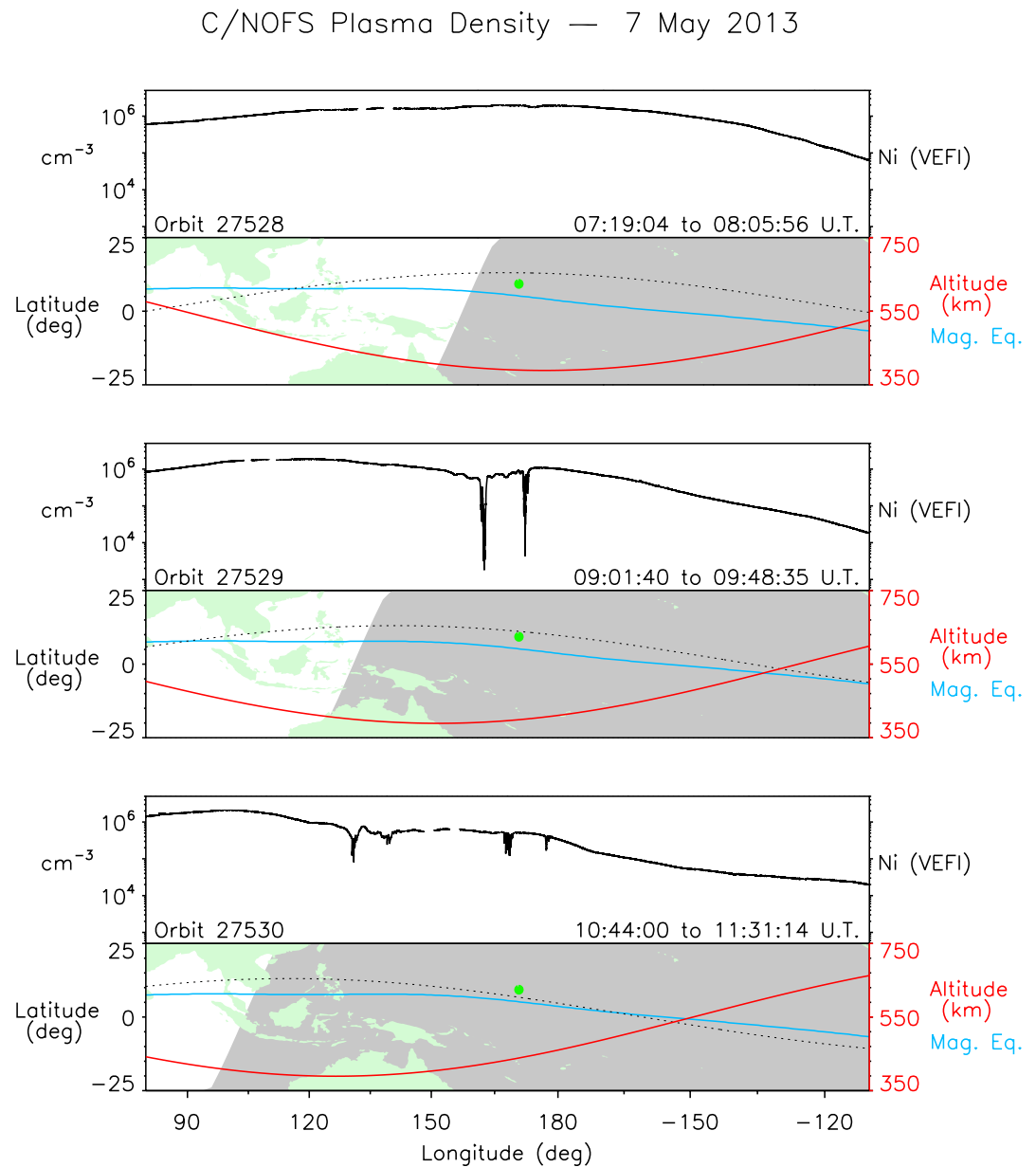
Figure 12. Plasma number density gathered during three consecutive passes of the Communications/Navigation Outage Forecasting System (C/NOFS) satellite over the western Pacific on 7 May 2013. The uppermost panel shows the density during the same orbit shown in Figure 11. The appearance of abrupt, narrow plasma depletions indicates the presence of spread-F instabilities. The bottom panel of each pass shows the geographic location and altitude of the satellite along with the green dot, indicative of the location of Kwajalein. Each successive pass is 102 s later. The gray shading shows the progression of the earth's shadow toward the west.

important feature of the plasma dynamics is that the zonal drift reversed direction at around 270 km, changing from eastward flow at higher altitudes to westward flow at the lower altitudes. This evidence of shear in the zonal plasma drift with altitude illustrates the changing circulation of the ionosphere during the sunset period which is at the core of the EVEX objectives. That the lower altitude plasma was traveling in the opposite zonal direction compared to that at higher altitudes underscores the importance of low altitude measurements and the pitfalls of extrapolating higher altitude satellite drift measurements to lower altitudes, particularly at low latitudes where the ambient magnetic field direction is largely horizontal.
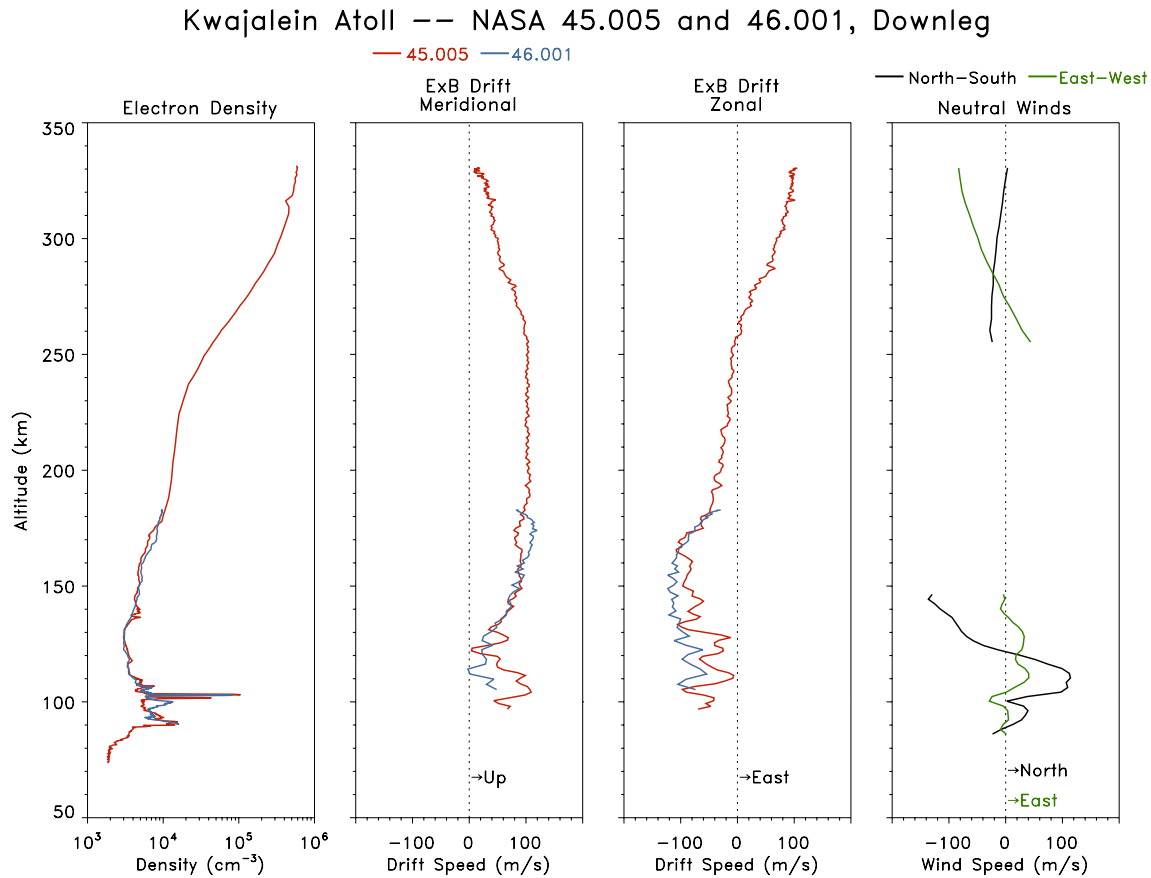
Figure 13. A composite presentation showing the plasma density and $\mathbf{E} \times \mathbf{B}$ plasma drift measurements plotted vs. altitude for the downleg trajectories of rockets 45.005 (blue) and 46.001 (red). The density data are shown in the left panel, the meridional drifts are shown in the second panel, and the zonal drifts are shown in the third panel. The fourth panel shows the neutral winds derived from the vapor trail measurements.

It is interesting that the observed zonal winds were largely oriented in the westward direction in the F-region and in the eastward direction in the lower E-region, opposite to the $\mathbf{E} \times \mathbf{B}$ drifts at these altitudes. In fact, this point is discussed at length in the companion article by Kudeki et al. On possible explanation, put forward by those authors, is that a local wind associated with a gravity wave might help explain the observations. Other considerations include the fact that the winds were reversing their direction at sunset and different time constants of the plasma response may contribute to the different directions observed for the winds and the ion motions.

The meridional drift profiles shown in Figure 13 reveal that the plasma was upgoing at all of the altitudes measured here, as discussed with respect to the same data shown in Figures 8 and 10. Importantly, the data reveal that this speed was not constant with altitude, but increased within the lower F-region and upper E-region (between 140 and 270 km), possibly associated with the lower plasma density within the emerging "valley" region. Note, however, that the vertical drifts lessened below about 140 km, where the plasma density actually reached their minimum values near 130 km. Referring again to Figure 2, we note again that the rockets were not in the same volume at the exact same times, so a comparison of the altitude profiles gathered with different rockets, such as shown in Figure 12, must be interpreted with care.

We can better appreciate the combined plasma drift data from the two rockets and C/NOFS by examining the changing $\mathbf{E} \times \mathbf{B}$ drifts along their different trajectories in an altitude-longitude format, as shown in Figure 14. The plasma drift data, illustrated here using arrow plots, reveal that the vertical plasma component is generally upwards along the entire trajectories of both rockets as well as along the C/NOFS trajectory. The arrow plot presentation shows that the zonal drifts on the high flyer rocket shift from eastward to westward flow below about 270 km on the downleg, as discussed above. The eastward drifts are present through the apogee region of the high
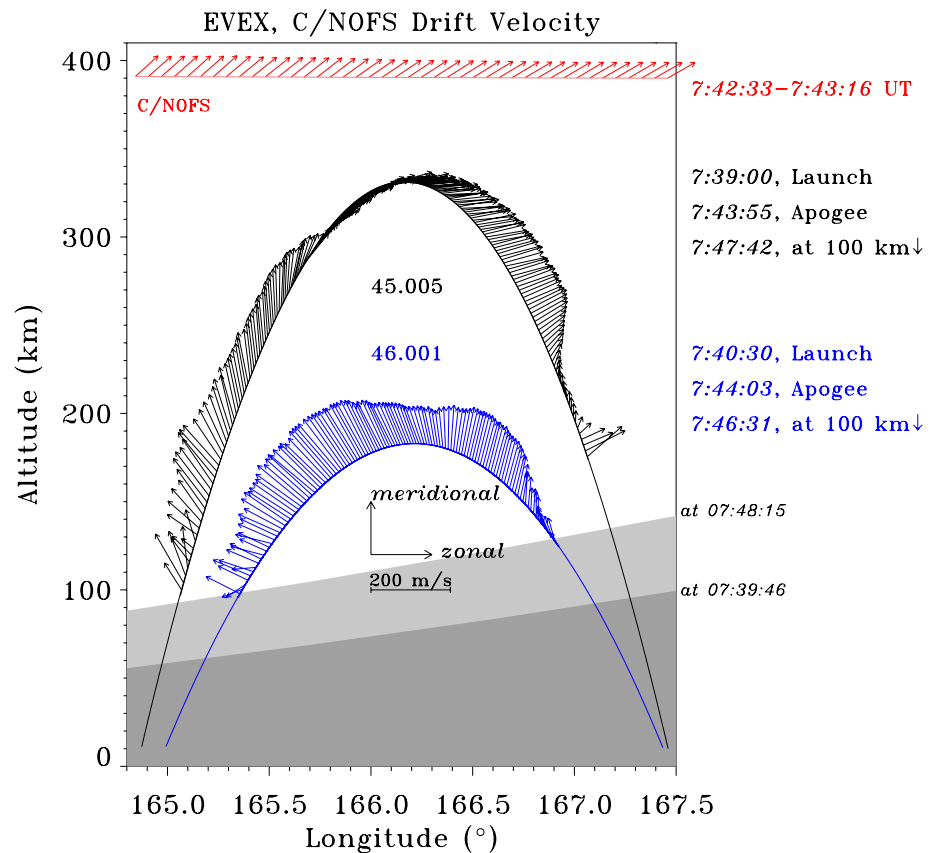
Figure 14. A composite presentation of the **E** × **B** plasma drift measurements, in an arrow display, along the trajectories of rockets 45.005 (black) and 46.001 (blue) as well as the C/NOFS satellite (red). The position of the earth's shadow is shown for two different times during the experiment for reference.

flyer, in accordance with the drifts measured by the C/NOFS satellite, as shown at the very top of Figure 14. Refer to the times indicated in Figure 2 for the exact temporal progression between the three platforms shown here.

It is interesting that the direction of the F-region zonal drifts did not reverse to westward on the upleg below 270 km, as they did on the downleg, although the zonal drift amplitudes diminished markedly below about 250 km altitude on the upleg to near zero values including a very brief interval of slightly westward flow around 200 km (see the very small upwards meridional electric fields in the top panel of Figure 7 near 130 s flight time). The low flyer upleg zonal drifts were eastward within the range of 150–177 km (see the downward meridional electric fields between 130 and 190 s in the upper panel of Figure 9), and then switched to westward drifts near apogee and throughout the downleg, in accordance with the westward drifts measured below 270 km along the high flyer downleg trajectory.

The general picture that has emerged from the simultaneous rocket and satellite measurements is that the large scale plasma drifts exhibited a complex, though organized, circulation pattern that changed with altitude and local time (longitude). When examining the drifts between the two rockets, we again emphasize that several minutes had transpired between their upleg and downleg and the ionosphere was rapidly changing in this narrow longitude region during sunset conditions, as discussed below.

6. E-Region "Valley" Ionosphere at Sunset

We now take a more detailed look at the lower ionosphere during this sunset period by examining the downleg observations of both rockets in the so-called "valley region" which corresponds to those altitudes between the increased lower E-region density and the F-region ledge. The plasma density from the two payloads on their downlegs are presented on the same altitude scale, between 80 and 180 km, in Figure 15. The right-hand panel
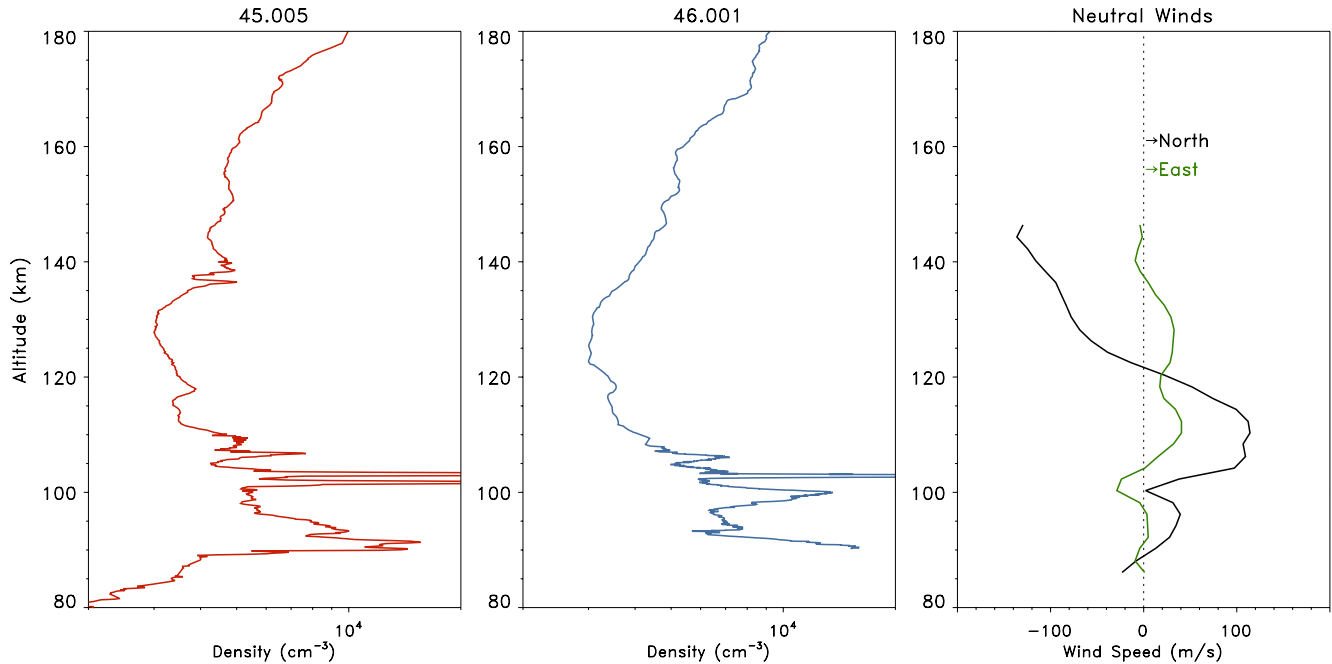
Figure 15. The plasma density gathered on the downleg of rockets 45.005 (left) and 46.001 (center) in the valley region of sunset ionosphere below the F-region ledge. The right-hand panel shows the neutral wind measurements discerned from the vapor trails.

shows the neutral wind velocity from the vapor trail experiment shown in Figure 13 released on a sub-payload that followed the same trajectory as the low flyer rocket (46.001).

For these downleg encounters, the two rockets were separated from each other by horizontal distances of about 50 km of, as shown in Figure 16, with the high flyer gathering data about 85 s after the low flyer within these downleg encounters.

Notice that the plasma density profile associated with the downleg of the rockets shows structures, especially near 140 km on rocket 45.005. These localized density increases observed on both rockets may be caused, in part, by the significant westward plasma flow that was strongest near these altitudes (see Figure 13). The local plasma density at these altitudes could also have been influenced by the increased southward-directed neutral winds with speeds as high as 140 m/s that were strongest at these same altitudes, as shown in the right-hand panel of Figure 15. Such equatorward winds can "push" the plasma up the slightly inclined (−9.8°) magnetic field against gravity, creating a density enhancement, as described by Kelley (2009) and illustrated schematically in Figure 17.

An important related observation is the appearance of strong sporadic-E layers evident on the downleg of each rocket at even lower altitudes, near 102 km, presumably due to metallic ions that are slow to recombine. Here, the amplitude of the density structures becomes significantly larger, with sharp edges defined by the multiple "sporadic-E" layers between 100 and 110 km. Such layers were even more pronounced in the downleg data from rocket 45.005 where two very large, sharp layers were observed with a vertical separation of only a few kilometers. The existence of sporadic-E layers and their significant variation (i.e., between a single and double layer) observed nearly simultaneously on two platforms with a horizontal separation of 50 km, underscores that the region was subject to strong variations in neutral winds and plasma density.

Finally, we comment on the shorter scale density structures (with scale sizes of 100's of meters to less than 1 m) that were present in the data below 110 km in the regions above and below the sporadic-E layers. These are shown in the sonograms of the density fluctuations ($\Delta N/N$) filtered above 10 Hz, plotted vs. altitude, for each rocket in Figure 18. The irregularities appear on the topside or bottomside of the different layers, indicative of drift waves driven by either the electric field or neutral wind, as discussed by Kagan and Kelley (1998). The amplitudes of the
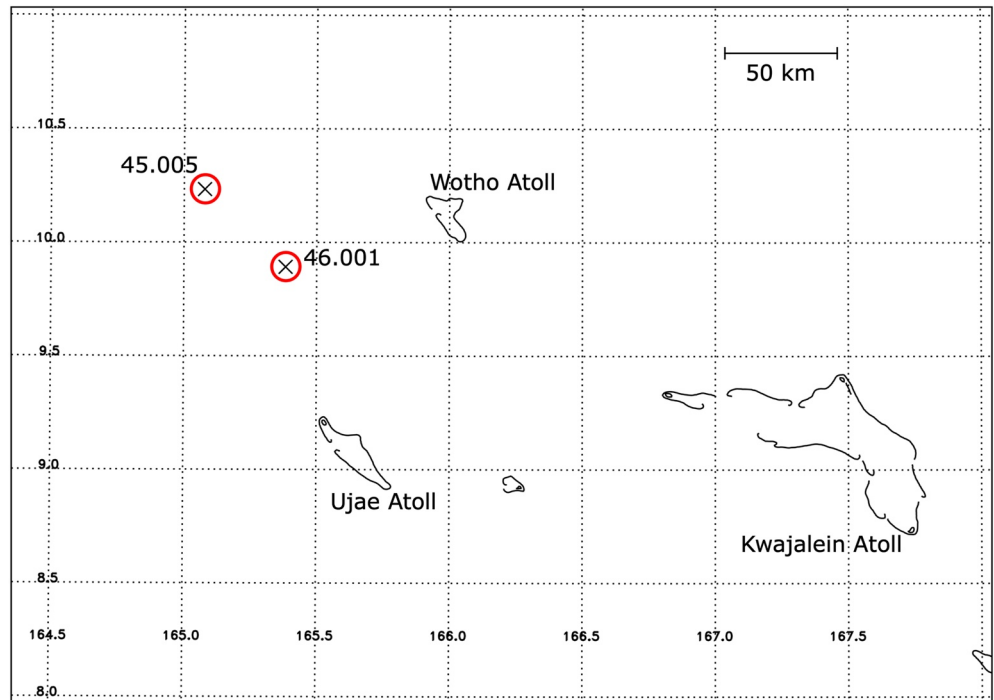
Figure 16. The location of the 45.005 and 46.001 payloads on their descent into the lower ionosphere for the measurements presented in Figure 15. The locations, depicted by the red circles, show the payload geographic locations while they were each at 102 km altitude on the downleg. At this time, their measurements were separated in time by 86 s.

short-scale irregularities are strongest in regions associated with the sharp sporadic-E layers and increased mobility within the altitudes of 100–110 km. The appearance of significant irregularities associated with the density layering is in agreement with the strong, coincident VHF backscatter radar echoes observed at these altitudes by the IRIS radar during this experiment (Kudeki et al., 2022).

To summarize this discussion, the plasma environment of the ionospheric valley region and lower E-region encountered by two simultaneous rockets launched into rapidly changing sunset conditions reveal a picture of very rich and diverse physical processes. Observations in the sunset valley region reveal significant variations of localized plasma density, suggesting a dynamic plasma population with large scale structures possibly driven by neutral wind shears associated sporadic-E layers at lower altitudes, and/or by gravity waves or plasma instabilities. The structured plasma environment in the valley region also has structured electric fields, as shown in Figure 13. Below this region (i.e., below about 110 km), a variable sporadic-E environment is observed which is the seat of shorter scale plasma density oscillations that appear to be the source of the 3 m backscatter echoes observed by the IRIS radar (Kudeki et al., 2022).

7. Discussion

7.1. Electrodynamics and the Sunset "Theater"

The EVEX experiment encompassed a highly dynamic, evolving low latitude ionosphere at sunset that is characterized by significant variations of plasma drifts and neutral winds. It is within this "theater" that the two EVEX rockets were launched, providing simultaneous observations along trajectories with apogees of 182 and 331 km in which data were gathered for 6–8 min and in which the lower atmosphere was in shadow while the ionosphere above was sunlit, yet on the verge of oncoming darkness. Since the rocket horizontal velocities were both westward and moving slightly faster than that of the earth's shadow, their trajectories kept the instrument probes largely within
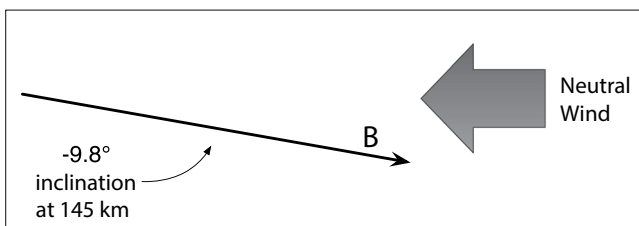

Figure 17. Illustration showing the magnetic field inclination within the ionosphere encountered by the payloads at 145 km altitude and the strong equatorward wind that was directed within the meridional plane that was largely aligned with the magnetic field direction.
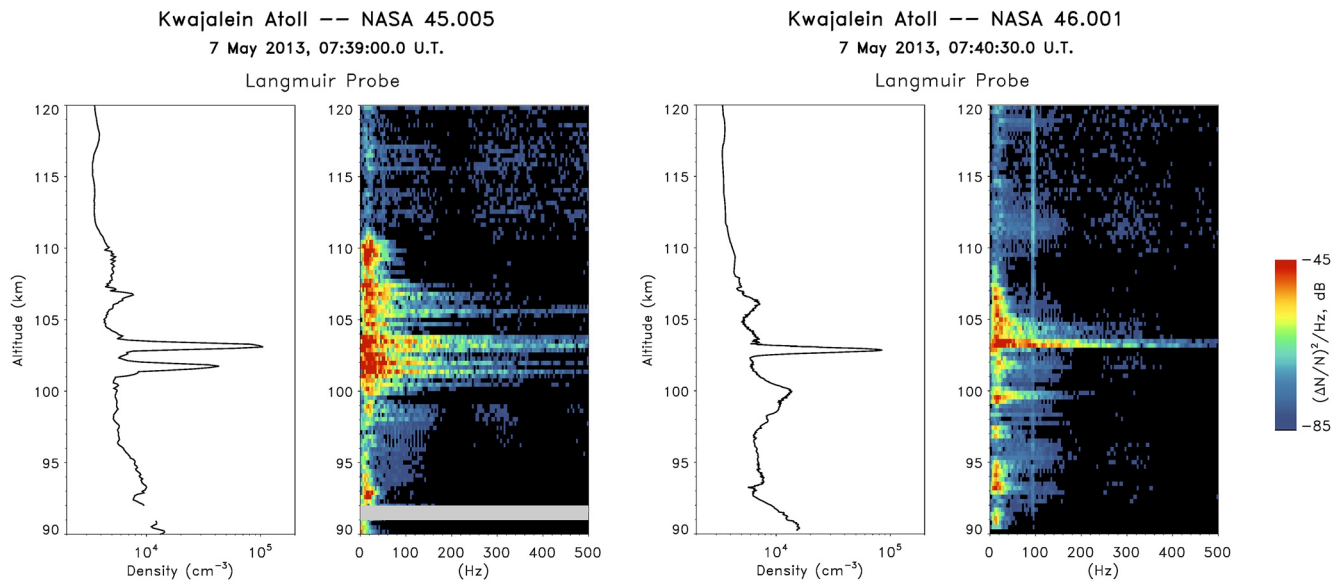
Figure 18. Spectrograms plotted vs. altitude of the plasma density variations (DN/N) measured with the Langmuir probe and filtered above 10 Hz on the downleg trajectories of payloads 45.005 and 46.001 between 90 and 130 km altitude. The payloads each encountered strong sporadic-E layers as depicted in the plasma density data on the left-hand panels for each rocket.

the sunset conditions for the majority of the data-taking portion of their sub-orbital flights. Furthermore, the C/NOFS satellite provided important, coincident measurements along an essentially horizontal eastward trajectory at a slightly higher altitude (390 km).

We seek to understand the *in situ* observations as descriptions of a rapidly changing equatorial ionosphere/thermosphere at sunset, evolving within a narrow range of longitudes over an interval of about 8 min duration. The background conditions are slowly varying within this period since the source of EUV ionization and heating disappears with the waning horizontal rays of the setting sun. Indeed, the variations of background, thermal ionosphere appear to be less consequential compared to the faster time scales upon which the region must adjust as a system to the highly dynamic plasma and neutral motions. Indeed, these variations with altitude and longitude were manifest on relatively short time and distance scales, given the fact that the upleg and downleg rocket trajectories were separated by time scales of minutes and distance scales of 1°–2° of longitude. For these reasons, the rocket observations underscore that the ionosphere at sunset should be considered as a multi-dimensional ensemble or theater, evolving in space and time that is subject to a rich, two-dimensional dynamical forcing, as opposed to a simple background ionosphere that unfolds linearly with respect to local time variations brought about by the changing solar zenith angle.

Understanding the equatorial ionosphere at sunset has received considerable theoretical and experimental attention for over half a century, ever since the earliest ionosonde and radar observations revealed that the equatorial ionosphere frequently rises at sunset. This augmented vertical plasma drift or pre-reversal enhancement results from an increase of the zonal electric field (e.g., Kelley, 2009) that has been considered as an important ingredient to explain the onset of subsequent evening instabilities including equatorial spread-F. Building on early fundamental research of equatorial ionospheric electrodynamics, for example, by Heelis et al. (1974) and Rishbeth (1971), the pre-reversal enhancement at sunset has been studied by numerous authors including Eccles (1998a), Farley et al. (1986), Haerendel et al. (1992), and Heelis et al. (2012). Although the details of the explanations may differ (see review by Eccles et al., 2015), in each case variations in the horizontal neutral wind at sunset are invoked as the key driving force for creating the necessary conditions to enable the zonal electric field to be enhanced and hence drive the sunset F-region ionosphere to higher altitudes.

In concert with studies of the pre-reversal enhancement, the next important concept to be introduced was the idea that a sunset vortex would evolve as a result of the changing horizontal and vertical motions within the sunset equatorial ionosphere. Originally put forward by Tsunoda et al. (1981) using evolving Altair backscatter echo structures as tracers, the first definitive evidence of equatorial plasma motions forming a vortex at sunset
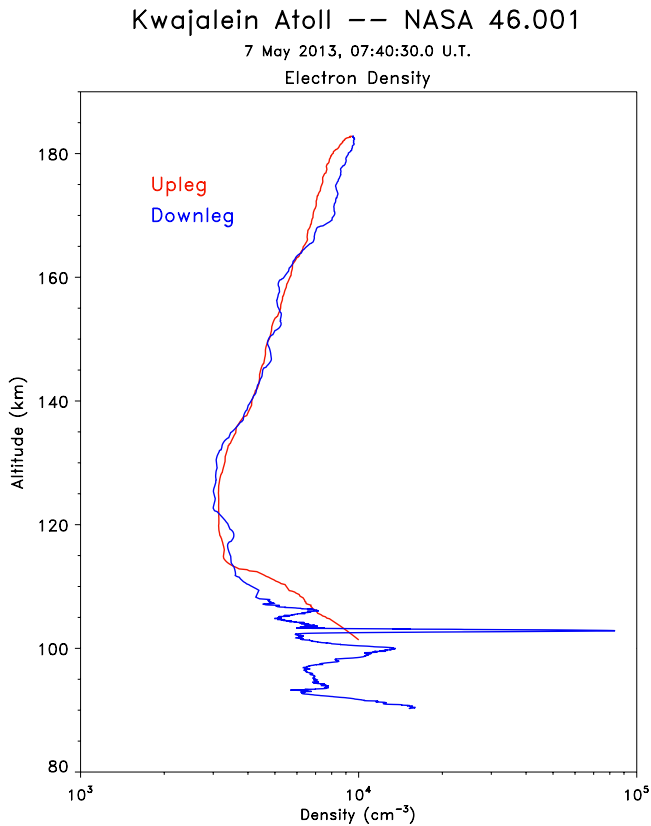
Figure 19. Plasma density measurements gathered on the low flyer payload (46.001) showing altitude profiles for the upleg and downleg traversals of the E-region.

came from Jicamarca radar observations reported by Kudeki and Bhattacharyya (1999). Eccles et al. (1999) used a composite of vector electric field observations from different orbits of the San Marco satellite to provide a picture of plasma drifts at sunset that resembled a vortex (see their Figure 4.) Important theoretical and modeling work has further advanced the idea of a vortex (e.g., Eccles, 1998a, 1998b, Eccles et al., 2015; Haerendel et al., 1992; Rodrigues et al., 2012). In particular, Rodrigues et al. (2012) has shown that the TIEGCM model reproduces the overall patterns of the vortex based on the E and F-region dynamos.

The combined rocket and radar observations of NASA's EVEX campaign provide an important new perspective of low latitude electrodynamics at the equator. In particular, the simultaneous observations from the two rockets launched in conjunction with radar, ionosonde, and satellite observations underscore the dynamic and evolving ionospheric system upon which we base our interpretations.

7.2. Evolving Neutral Winds and Electric Fields at Sunset

To set the stage for the evolving plasma and neutral motions, we return to the plasma number density measured vs. altitude. The plasma density measurements, shown on the left-hand panel of Figure 8 and enlarged in Figure 19, clearly show that the measured E-region plasma were similar on both the upleg and downleg and were significantly reduced compared to typical daytime plasma density values. In addition to the *in situ* plasma density measurements, simultaneous radar and ionosonde data also show that the conductivity of the lower ionosphere was substantially reduced during the sunset conditions that are the subject of the investigation reported here. Surprisingly, however, the plasma density observed along the rocket trajectories reveal that on the western edge of the narrow region under study (downleg trace in Figure 19), the plasma density was considerably more structured than on the eastern region (upleg trace), despite the fact that the westward region corresponded to slightly *earlier* local times when recombination effects would be slightly less pronounced. This enhanced structure may have resulted from the significant plasma and neutral dynamics that were more active within the western flank, revealed in particular by data from the electric field probes on both rockets as they encountered the western region of the ionosphere on their downlegs. Local neutral wind forcing, perhaps associated with gravity waves, could affect the plasma density, as discussed in the previous section, and provide a reasonable explanation of the very different E-region plasma density profiles.

Within this plasma number density environment, both the observed winds and $\mathbf{E} \times \mathbf{B}$ drifts show very dynamic signatures, evolving in altitude and within a narrow local time (longitude) extent. The neutral wind measurements are available from the vapor trail experiments reported by Kiene et al. (2015). The upper atmosphere motions observed in the vapor trail data between 250 and 330 km obtained about 10 min after the rocket launches revealed a shear in the zonal wind flow, from westward to eastward with decreasing altitude. Importantly, continuous observations of the vapor trails from which the winds were derived showed that their zonal velocity was dramatically reduced at these same altitudes after 21 min from the initially reported observations at 7:50 UT to those at 8:11 UT (see Figure 4 of Kudeki et al., 2022).

In tandem with the observations of varying neutral winds, observations from both rocket payloads reveal strong zonal $\mathbf{E} \times \mathbf{B}$ drifts that vary with both altitude and longitude (i.e., between the rocket upleg and downleg trajectories.) The zonal plasma drifts clearly show differences between the eastern flank (later LT from upleg data) and western flank (earlier LT from downleg data) as shown in right-hand panels of Figures 8 and 10. The downleg of the high-altitude rocket showed a clear change from westward to eastward zonal drifts near 270 km. The C/NOFS data (Figure 11) showed that this change occurred somewhat earlier at a higher altitude (near 400 km), which is the customary local time of the zonal drift reversal in the late afternoon in the F-region as observed on C/NOFS and other satellites (e.g., Coley et al., 2014; Fejer et al., 2013). Furthermore, as shown in the right-hand panel of

Figure 8, the high altitude rocket's upleg data showed eastward drifts that were decreasing in magnitude at lower altitudes (220–250 km) becoming near zero and even slightly westward at 220 km before turning back eastward at lower altitudes below about 190 km. This is dramatic evidence of shears in the horizontal plasma motions that were varying within a narrow altitude range.

The EVEX observations of reversals of the zonal drift as a function of altitude provide important new information because they are observed at and below the F-region ledge and because their variations were observed within a very narrow horizontal distance corresponding to a few degrees of longitude. Using sounding rocket measurements, Hysell et al. (2005) also reported reversed zonal drifts at the base of the F-region ledge yet at later local times. Those authors associated this shear with the conditions responsible for the onset of spread-F observed by the Altair radar. Using C/NOFS satellite observations near perigee when the F-region became elevated at sunset, Pfaff (2015) reported shear with altitude of the zonal plasma drift and also related this to the onset of observed large scale instabilities.

At later local times corresponding to the eastern regions of the ionosphere, the direction of the observed horizontal drifts shifts to eastward flow on both rockets, as shown by the $\mathbf{E} \times \mathbf{B}$ drifts from the uplegs of the two rockets (see right-hand panels of Figures 8 and 10) as well as the composite data presentation shown in Figure 14. These eastward drifts at the later local time are consistent with the overall nighttime circulation in which the ionosphere plasma drifts eastward at all altitudes into the night. In contrast, at the earlier local times corresponding to the western flank of the sunset region studied in this experiment, the rocket downleg data shows strong westward flow at the lower altitudes (below 200 km) consistent with the Altair E-region radar measurements, discussed in the companion article, Kudeki et al. (2022).

We now consider the zonal electric fields and their associated *vertical* plasma motion. The electric field probes on both rockets measured eastward zonal electric fields at all altitudes along their trajectories associated with upwards (meridional) $\mathbf{E} \times \mathbf{B}$ plasma drifts. Despite their constant direction, the magnitude of these eastward electric fields varied significantly with altitude as well as with local time.

As shown in the middle panel of Figure 8, notice how the vertical drift (zonal electric fields) are enhanced on both the upleg and the downleg in the region between 150 and 250 km, coincident with the lower background thermal plasma density below the F-region ledge. Notice, however, that the vertical plasma drifts are increased by over a factor of about 3 or 4 on the downleg (western region) compared to the upleg, even though the plasma density did not change by a corresponding amount between the upleg and downleg. This observation shows that the electric field variations are not governed by changes in the ambient density, but, rather, are controlled by larger scale, dynamic processes that ensure plasma flow continuity with respect to both altitude and local time. For reference, the time between the upleg and downleg traversals of when the trajectory of this rocket encountered 180 km altitude is 6 min.

For this experiment, the increase in the altitude of the F-peak for this sunset period was very modest, as indicated by the hmF2 altitude variations in the ionosonde data (see Kudeki et al., 2022). This is also consistent with the plasma density measured by the C/NOFS satellite which did not show any significant increase of the density along its horizontal trajectory, or any evidence that the F-region ledge had risen above the satellite altitude of 390 km. Although the ionosonde data show that the pre-reversal "enhancement" of the F-region peak was moderate, the rocket observations reveal that the vertical drifts were nevertheless quite pronounced at the lower altitudes below the F-region ledge.

Our measured vertical drifts are consistent with Jicamarca radar observations of the altitude dependence of F-region vertical plasma drifts reported by Fejer et al. (2014). Those authors showed that over a course of 5–10 min, the vertical drifts could increase by a factor of two. They also showed the preponderance for the vertical drifts to be larger at the lower altitudes, particularly between 200 and 400 km. (The radar measurements reported in Fejer et al., 2014 did not show data below 200 km.) In general, the vertical drifts measured by the rockets reported here are higher (by about a factor of 2) compared to the vertical drifts measured by the Jicamarca radar. This difference could be due to geophysics or longitude effects, or perhaps uncertainties in the measurement.

Importantly, it is not at all surprising that the zonal electric fields (and hence the upwards drift velocities) would be modulated as a result of the variations in the horizontal drifts (driven by the winds) in order to keep the plasma flow continuous, essentially to maintain $\nabla \times \mathbf{E} = 0$, a requirement emphasized by Eccles et al. (2015).
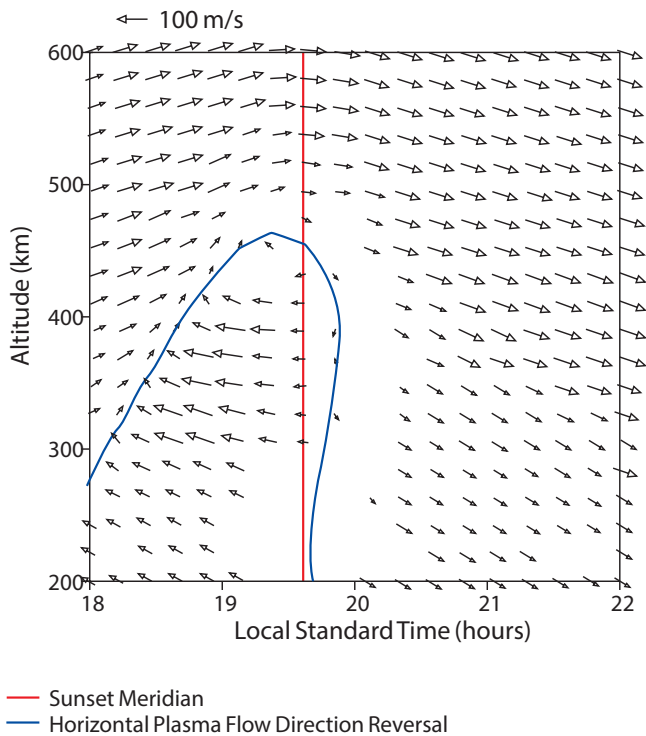
Figure 20. Model results from Haerendel et al. (1992) showing the existence of a plasma vortex in the ionosphere at the earth's magnetic equator at sunset. The thin solid line corresponds to the reversal of the zonal plasma drift.

Indeed, the vertical drift amplitudes are largest on the downleg (western flank) when the zonal drifts are undergoing pronounced shear and the plasma density is decreased. Thus, to maintain $\nabla \times \mathbf{E} = 0$ and that the divergence of the currents be zero, these altitudes are precisely where we would expect increased vertical currents and plasma flow. Eventually, at a somewhat later time, the zonal electric field is expected to reverse direction and drive the plasma downwards, as indicated in the C/NOFS electric field measurements near 7:46 U.T. at altitudes near 400 km in Figure 11.

Modeling results by Haerendel et al. (1992) reproduced in Figure 20 show the vertical plasma drift shifting from upwards to downward after sunset. More importantly, the simulation shows the horizontal plasma drift shifting from eastward to westward at lower altitudes (here, below 400 km) just prior to sunset in a manner similar to the rocket observations presented here, particularly those gathered along the downleg trajectories in the western flank of the sunset theater. Furthermore, the simulation shows the zonal drift reversal is not symmetric but changes its abruptness and character as a function of altitude and local time between the western and eastern flanks organized by the sunset meridian. Eventually, the zonal plasma drifts in the simulation are eastward at all altitudes at the later (post-sunset) local times which is consistent with the overall nighttime circulation in which the ionospheric plasma drifts eastward into the night.

To conclude the discussion, the rocket measurements clearly show that there was a complex, though organized, electrodynamics evolving at sunset on 7 May 2013 in the ionosphere to the west of Kwajalein Atoll. This sunset theater was characterized by highly dynamic $\mathbf{E} \times \mathbf{B}$ plasma drifts and neutral winds that varied with altitude and longitude. The overall picture is one marked with both east-west shears and plasma rising at variable speeds depending on altitude, consistent with the fact that the plasma flow must be continuous.

Ultimately, the plasma drifts are coupled to the neutral winds and governed by the requirement that the $\nabla \times \mathbf{E} = 0$ and that the divergence of their combined, associated currents be zero.

8. Conclusions

The main results revealed by the probe measurements carried out as part of the simultaneous dual sounding rocket EVEX experiment in conjunction with a coincident C/NOFS satellite perigee pass are as follows:

1. When observations are combined from three independent measurement platforms, the $\mathbf{E} \times \mathbf{B}$ plasma drift data reveal highly variable plasma flow patterns in both altitude and local time within a very narrow longitude region at sunset in the near-equatorial ionosphere

2. The meridional or vertical plasma drift was at all times and altitudes upwards, although the magnitude of the vertical drift was not constant, increasing in the upper valley region between 140 and 250 km altitude. These vertical drifts were largest below the F-region ledge where the plasma density was generally low, although their significant increase in amplitude on the downleg (western flank of the observing theater) did not correspond to a further decrease in the ambient plasma density in this region

3. The zonal plasma drifts shifted from eastward to westward-directed flow at the western flank of the sunset region, producing a shear with altitude in the zonal plasma flow at 270 km

4. The strong westward-directed plasma below the F-region on the western flank was observed coincident with the larger upward plasma velocity, consistent with the maintenance of plasma flow including vortex-like circulation

5. The strong eastward plasma flow at the eastern flank of the sunset region is consistent with the larger scale eastward circulation of the nighttime ionosphere. The shift from westward to eastward flow on the sides of the sunset region is consistent with theoretical modeling work published by Haerendel et al. (1992)

6. Coincident electric field and plasma density observations gathered during an overfly of the C/NOFS satellite not only completed the electrodynamic picture within the F-region at somewhat higher altitudes, but also underscore how satellite observations at these altitudes do not capture the highly dynamic ionosphere at the lower altitudes which are so important for establishing the plasma and neutral dynamics and to set the stage for the initiation of spread-F instabilities. Subsequent C/NOFS orbits revealed the presence of spread-F depletions which were consistent with those observed with the Altair radar

7. Surprisingly, the plasma density on the western flank of the narrow region under study revealed considerable more structure than on the eastern flank, despite the fact that the western portion corresponded to slightly earlier local times. For example, plasma density variations were observed on both rockets in the E-region valley between 135 and 155 km which was coincident with larger amplitude plasma motion variations and a significant equatorward neutral wind with speeds over 140 m/s

8. The combined data set reveals a picture of a highly evolving, dynamic plasma and neutral gas environment which varies on short time and distance time scales. These observations underscore that the ionosphere at sunset must be considered as a multi-dimensional ensemble of interconnected flows and vortices encompassing an evolving theater of spatial and temporal variations, as opposed to a background that simply unfolds linearly with respect to local time and the changing solar zenith angle. Such plasma motions may be expected to enable large scale plasma instabilities to form, as was observed later in the night over Kwajalein by the C/NOFS satellite as well as by both the Altair and IRIS radars, as discussed in the lead article (Kudeki et al., 2022)

The EVEX data set is unique in that it presents the first sounding rocket measurements of electrodynamics and neutral winds in the E- and F-region ionosphere at sunset. Accordingly, it opens a window that reveals highly complex, yet organized, plasma drifts, winds, and density variations that exist in the lower altitudes of the terminator theater of the earth's low latitude ionosphere/thermosphere. It is this highly dynamic environment that sets the stage for a number of fundamental plasma processes that subsequently arise as the equatorial ionosphere evolves into the night.

Appendix A: Impedance Probe Measurements

Each EVEX rocket payload included an impedance probe built and tested at the Goddard Space Flight Center to provide, among other parameters, the absolute plasma density. The probes functioned well on each rocket, providing resonances that varied as the ambient density changed along the trajectories. Below, we present results from the impedance probe on the high flyer rocket (45.005) as it gives an excellent independent indication of the plasma density encountered along that rocket's trajectory.

A1. Brief Description of Probe

Goddard has developed a wideband impedance probe to measure absolute plasma densities in conjunction with the Langmuir probe (Rowland et al., 2011). This impedance probe has been flown on a number of sounding rockets with different apogees launched at different latitudes. The probe consists of a system of electrodes that stimulate the plasma with a white noise signal containing frequencies from 10 kHz to several MHz. The impedance probe measures the voltage drop in the two legs of a voltage divider while the white noise is applied: one that contains a reference impedance and the other that consists of the impedance of the electrodes in the plasma. For each white noise burst, these voltage drops are telemetered to the ground as time series where they are converted into the ratio of the reference impedance to the plasma impedance as a function of frequency. Since the reference impedance is known, this allows a measure of the complex impedance of the plasma at all frequencies covered by the white noise spectrum simultaneously. Several parameters of physical interest can be derived from the complex impedance as a function of frequency (e.g., Jensen & Baker, 1992). In particular, the "parallel resonance" occurs at the upper hybrid frequency, allowing a determination of the electron number density since the magnetic field is known from models and measurements. In addition, at lower frequencies, a "series resonance" can sometimes be observed in the data which contains information about the electron temperature.

The impedance probe flown on the EVEX payloads gathers resonances and hence plasma density measurements approximately every 136 ms. The frequencies correspond to plasma densities that range from 10^2 to 10^6 cm^{-3}.

A2. Results From Rocket 45.005

Figure A1 shows data from the GSFC impedance probe from EVEX rocket 45.005. The display shows the normalized antenna impedance as a function of flight time and frequency. The normalized impedance is the measured impedance divided by the "free-space" impedance at altitudes below 85 km where the plasma density is very low.

The data show strong plasma resonances throughout the entire flight, corresponding to both the E- and F-region ionosphere. Notice that the shape of the resonance is generally symmetric about apogee between the upleg and downleg. The notch near 350 s flight time (320 km on the downleg) corresponds to when the Lithium vapor trail was released and is not geophysical. The E-region ionosphere below 200 km altitude encountered after about 460 s flight time shows considerable structure as was also apparent in the Langmuir probe data and discussed in the main article. The white dotted line corresponds to the local electron gyro frequency which was below the plasma frequency for almost the entire flight.

The maximum resonance occurred at apogee near 5 MHz. Assuming this resonance is the upper hybrid frequency, this resonance corresponds to a plasma density of 3×10^5/cc at the apogee location of this rocket. Comparisons with the Langmuir probe data and ionosonde indicate that the plasma density provided by this straightforward analysis of the impedance probe resonances underestimated the true plasma density by about a factor of 2. Accordingly, as explained in the main text, we normalized the Langmuir probe data at apogee to the density derived from the ionosonde and used those plasma density profiles in the analysis presented herein. Nevertheless, the impedance probe data were exceedingly useful for providing an independent measure of the plasma density including its variations along the flight path, particularly below 200 km altitude on the downleg.
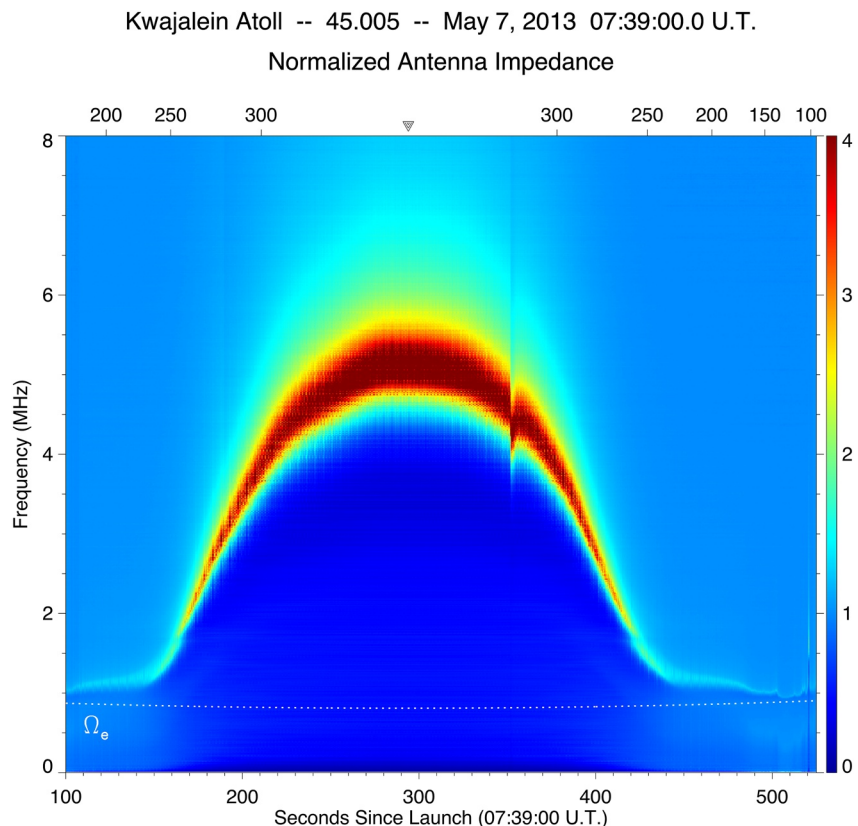

Figure A1. Plasma resonances observed with the impedance probe on rocket 45.005. The dotted line corresponds to the electron gyro frequency.

Conflict of Interest

The authors declare no conflicts of interest relevant to this study.

Data Availability Statement

The rocket data supporting this article are publicly available via Zenodo. The link to the data set on Zenodo is: https://doi.org/10.5281/zenodo.6127528.

References

Coley, W. R., Stoneback, R. A., Heelis, R. A., & Hairston, M. R. (2014). Topside equatorial zonal ion velocities measured by C/NOFS during rising solar activity. *Annales Geophysicae*, *32*(2), 69–75. https://doi.org/10.5194/angeo-32-69-2014

Eccles, J. V. (1998a). Modeling investigation of the evening prereversal enhancement of the zonal electric field in the equatorial ionosphere. *Journal of Geophysical Research: Space Physics*, *103*(A11), 26709–26719. https://doi.org/10.1029/98JA02656

Eccles, J. V. (1998b). A simple model of low-latitude electric fields. *Journal of Geophyical Research*, *103*(A11), 26699–26708. https://doi.org/10.1029/98ja02657

Eccles, J. V., Maynard, N., & Wilson, G. (1999). Study of the evening plasma drift vortex in the low-latitude ionosphere using San Marco electric field measurements. *Journal of Geophysical Research: Space Physics*, *104*(A12), 28133–28143. https://doi.org/10.1029/1999ja900373

Eccles, J. V., St. Maurice, J. P., & Schunk, R. W. (2015). Mechanisms underlying the prereversal enhancement of the vertical plasma drift in the low-latitude ionosphere. *Journal of Geophysical Research: Space Physics*, *120*(6), 4950–4970. https://doi.org/10.1002/2014JA020664

Farley, D. T., Bonelli, E., Fejer, B. G., & Larsen, M. F. (1986). The prereversal enhancement of the zonal electric field in the equatorial ionosphere. *Journal of Geophysical Research: Space Physics*, *91*(A12), 13723–13728. https://doi.org/10.1029/JA091iA12p13723

Fejer, B. G., Farley, D. T., Gonzales, C. A., Woodman, R. F., & Calderon, C. (1981). F-region east-west drifts at Jicamarca. *Journal of Geophysical Research: Space Physics*, *86*(A1), 215–218. https://doi.org/10.1029/JA086iA01p00215

Fejer, B. G., Hui, D., Chau, J. L., & Kudeki, E. (2014). Altitudinal dependence of evening equatorial F-region vertical plasma drifts. *Journal of Geophysical Research: Space Physics*, *119*(7), 5877–5890. https://doi.org/10.1002/2014JA019949

Fejer, B. G., & Scherliess, L. (2001). On the variability of equatorial F-region vertical plasma drifts. *Journal of Atmospheric and Solar-Terrestrial Physics*, *63*(9), 893–897. https://doi.org/10.1016/s1364-6826(00)00198-x

Fejer, B. G., Tracy, B. D., & Pfaff, R. F. (2013). Equatorial zonal plasma drifts measured by the C/NOFS satellite during the 2008–2011 solar minimum. *Journal of Geophysical Research: Space Physics*, *118*(6), 3891–3897. https://doi.org/10.1002/jgra.50382

Haerendel, G., Eccles, J. V., & Çakir, S. (1992). Theory for modeling the equatorial evening ionosphere and the origin of the shear in the horizontal plasma flow. *Journal of Geophysical Research*, *97*(A2), 1209. https://doi.org/10.1029/91ja02226

Heelis, R. A., Crowley, G., Rodrigues, F., Reynolds, A., Wilder, R., Azeem, I., & Maute, A. (2012). The role of zonal winds in the production of a pre-reversal enhancement in the vertical ion drift in the low latitude ionosphere. *Journal of Geophysical Research: Space Physics*, *117*(A8), A08308. https://doi.org/10.1029/2012JA017547

Heelis, R. A., Kendall, P. C., Moffeit, R. J., Windle, D. W., & Rishbeth, H. (1974). Electrical coupling of the E- and F-regions and its effect on F-region drifts and winds. *Planetary and Space Science*, *22*(5), 743–756. https://doi.org/10.1016/0032-0633(74)90144-5

Hysell, D. L., Larsen, M. F., Swenson, C. M., Barjatya, A., Wheeler, T. F., Sarango, M. F., et al. (2005). Onset conditions for equatorial spread F determined during EQUIS II. *Geophysical Research Letters*, *32*(24). https://doi.org/10.1029/2005GL024743

Jensen, M. D., & Baker, K. D. (1992). Measuring ionospheric electron density using the plasma frequency probe. *Journal of Spacecraft and Rockets*, *29*(1), 91–95. https://doi.org/10.2514/3.26318

Kagan, L. M., & Kelley, M. C. (1998). A wind-driven gradient drift mechanism for mid-latitude E-region ionospheric irregularities. *Geophysical Research Letters*, *25*(22), 4141–4144. https://doi.org/10.1029/1998GL900123

Kelley, M. C. (2009). *The Earth's ionosphere: Plasma physics and electrodynamics*, *International Geophysical Series* (2nd ed., Vol. *96*). Academic.

Kiene, A., Larsen, M. F., & Kudeki, E. (2015). Equatorial F-region neutral winds and shears near sunset measured with chemical release techniques. *Journal of Geophysical Research: Space Physics*, *120*(10), 9004–9013. https://doi.org/10.1002/2015JA021462

Kudeki, E., Akgiray, A., Milla, M., Chau, J. L., & Hysell, D. L. (2007). Equatorial spread-F initiation: Post-sunset vortex, thermospheric winds, gravity waves. *Journal of Atmospheric and Solar-Terrestrial Physics*, *69*(17–18), 2416–2427. https://doi.org/10.1016/j.jastp.2007.04.012

Kudeki, E., & Bhattacharyya, S. (1999). Postsunset vortex in equatorial F-region plasma drifts and implications for bottomside spread-F. *Journal of Geophysical Research: Space Physics*, *104*(A12), 28163–28170. https://doi.org/10.1029/1998ja900111

Kudeki, E., Reyes, P., Wallace, A., Ye, B., Pfaff, R. F., Larsen, M. F., & Groves, K. M. (2022). A study of post-sunset spread-F initiation during the 2013 EVEX Campaign. *Journal of Geophysical Research: Space Physics*, *127*, e2021JA030256. https://doi.org/10.1029/2021JA030256

Pfaff, R. (2015). C/NOFS Observations of Reversed Zonal E × B Drifts Below the Equatorial Ionospheric F-Peak at Sunset and Their Implications for the Generation of Large Scale Instabilities. Presented at the 2015 AGU Fall Meeting, Retrieved from https://agu.confex.com/agu/fm15/webprogram/Paper61054.html

Pfaff, R., Rowland, D., Freudenreich, H., Bromund, K., Le, G., Acuña, M., et al. (2010). Observations of DC electric fields in the low-latitude ionosphere and their variations with local time, longitude, and plasma density during extreme solar minimum. *Journal of Geophysical Research: Space Physics*, *115*(12). https://doi.org/10.1029/2010JA016023

Rishbeth, H. (1971). Polarization fields produced by winds in the equatorial F-region. *Planetary and Space Science*, *19*(3), 357–369. https://doi.org/10.1016/0032-0633(71)90098-5

Rodrigues, F. S., Crowley, G., Heelis, R. A., Maute, A., & Reynolds, A. (2012). On TIE-GCM simulation of the evening equatorial plasma vortex. *Journal of Geophysical Research: Space Physics*, *117*(A5), A05307. https://doi.org/10.1029/2011JA017369

Rowland, D. E., Collier, M. R., Sigwarth, J. B., Jones, S. L., Hill, J. K., Benson, R., et al. (2011). Science of opportunity: Heliophysics on the FASTSAT mission and STP-S26. In 2011 *Aerospace Conference* (pp. 1–12). https://doi.org/10.1109/AERO.2011.5747235

Tsunoda, R. T., Livingston, R. C., & Rino, C. L. (1981). Evidence of a velocity shear in bulk plasma motion associated with the post-sunset rise of the equatorial F-layer. *Geophysical Research Letters*, *8*(7), 807–810. https://doi.org/10.1029/GL008i007p00807